Functional Implications of the Proximal Hydrogen-Bonding Network in Myoglobin: A Resonance Raman and Kinetic Study of Leu89, Ser92, His97, and F-Helix Swap Mutants†

Eric S. Peterson‡ and Joel M. Friedman*

Department of Physiology and Biophysics, Albert Einstein College of Medicine, Bronx, New York, 10461

Ellen Y. T. Chien and Stephen G. Sligar*

Department of Biochemistry and the Beckman Institute for Advanced Science and Technology, University of Illinois at Urbana-Champaign, 405 North Mathews Avenue, Urbana, Illinois, 61801

Received April 2, 1998; Revised Manuscript Received June 29, 1998

ABSTRACT: Resonance Raman spectra have been obtained for both the equilibrium deoxy derivative and the 10 ns photoproduct of the CO derivative of several mutants of sperm whale myoglobin. The particular mutations on the F-helix were chosen to expose the role of the proximal hydrogen-bonding network in maintaining the position of the heme, the proximal histidine, and the heme-7-propionate. In each mutant, one or more hydrogen bonds are altered or eliminated. A careful comparison of the spectra from the equilibrium and transient five coordinate species indicates that the tertiary relaxation after photodissociation is nearly complete within 10 ns, as is the case in the WT protein. The iron−proximal histidine stretching mode (ν(Fe−His)) and several low-frequency propionate-sensitive modes in the Raman spectra reveal the impact of specific disruptions in the hydrogen-bonding network on the heme pocket geometry. Two categories of perturbation are observed with respect to ν(Fe−His): (1) a shift in the peak frequency without a change in line shape and (2) changes in the overall line shape which may or may not be accompanied by a frequency shift. The alterations in the ν(Fe−His) band are interpreted as arising from conformational heterogeneity and local geometrical changes within the pocket, including movement of the heme group, and are discussed in terms of changes in the population distribution as revealed via a curve-fitting analysis. None of the frequency shifts in the ν(Fe−His) band are as large as that reported for the His93Gly(imidazole) mutant, suggesting that the covalent linkage between the heme and His93 plays a crucial role in maintaining the geometry of the proximal pocket. Molecular modeling indicates that the ν(Fe−His) frequency shifts observed in the present study originate from changes in the His93 imidazole ring azimuthal angle. The systematic variations in the interactions of the heme-7-propionate in the mutants have exposed several properties of the propionate-sensitive Raman bands. The frequencies of ν_9 (the 240 cm^{-1} shoulder on the ν(Fe−His) band) and $\delta(c_\beta c_c c_d)$ at ∼370 cm^{-1} appear to be correlated. A decrease in hydrogen-bond strength to this propionate in response to changes in stereochemistry or degree of disorder is associated with a decrease in the frequency of both ν_9 and $\delta(c_\beta c_c c_d)$. The mutations that cause a weakening of the hydrogen bonding to the heme-7-propionate also result in changes in ν(Fe−His) which are interpreted as evidence that this propionate participates in the anchoring of the heme within the heme pocket. Changes in γ_7 at ∼300 cm^{-1}, γ_6 at ∼335 cm^{-1}, and ν_8 at ∼342 cm^{-1} are discussed in terms of pocket disorder. A titration from pH 5.1 to 7.4 suggests that His97 is protonated in the WT protein by pH 5.1. Geminate-rebinding studies on these mutants indicate that disruption of the hydrogen-bonding network has only modest effects on ligand-binding kinetics, suggesting that the role of the hydrogen-bonding network may be one of maintaining heme pocket stability rather than of specific protein function.

Ligand binding to myoglobin and hemoglobin has long been used as a model system for the study of structure−function relationships in proteins. These proteins are of interest both as models of general protein behavior and in and of themselves as biologically important systems. A vast wealth of data now exists on wild-type proteins and various mutants in the form of X-ray crystal structures; ligand-binding kinetics; spectroscopic characterization of deoxy, ligated, and intermediate species; and theoretical modeling of the reaction coordinate potential surfaces. Despite this vast database, it is still not completely clear which residues in the protein are involved in ligand binding or which ones

† This work was funded by grants from the W. M. Keck Foundation (J.M.F.) and the NIH RO1-GM44343 (J.M.F.) and PO1HL51084 (J.M.F. and S.G.S.).

* Corresponding Authors. Friedman: tel, (718) 430-3591; fax, (718) 430-8819; e-mail, jfriedma@aecom.yu.edu. Sligar: tel, (217) 244-7395; fax, (217) 244-7100; e-mail, s-sligar@uiuc.edu.

S0006-2960(98)00752-1 CCC: $15.00
Published on Web 08/15/1998

modulate the binding affinity. Much work has been done in understanding the interactions between the residues in the distal pocket and O_2, CO, NO, and other small ligands (*1*−*12*). These studies demonstrate that mutations on the distal side of the heme pocket can cause large changes in the ligand-binding kinetics. In contrast, much less has been done on the proximal side. The proximal mutations that have been characterized have produced changes in the protein reactivity that are typically much less dramatic than those observed in the distal mutants.

Several models have been put forth in which the barrier to ligand binding is controlled by "proximal" strain in the covalent bond between the proximal histidine residue in the F-helix of the globin and the heme prosthetic group (*13*−*17*). In hemoglobin the F-helix moves more than 1.0 Å upon ligand binding during the T to R quaternary transition (*18*). Consequently, it is easy to implicate this large change in structure with the T/R dependence on binding affinity. It is much less apparent what controls affinity in Mb.[1] Comparison of X-ray structures of deoxy Mb (*19*) and carbonmonoxy Mb (*20*) shows that the F-helix in Mb is displaced by about 0.1 Å when the protein goes from CO ligated to deoxy form. An extensive hydrogen-bonding network present on the proximal side of the heme pocket in Mb, but not in Hb, is implicated in stabilizing the Mb proximal geometry (Figure 1a) (*21*−*23*). The N_δ proton of the proximal His93(F8) is H-bonded to the backbone carbonyl of Leu89(F4) and to the O_γ of Ser92(F7). In addition, the carboxylate group of the heme-7-propionate is H-bonded to the His97(FG3) imidazole ring and the hydroxyl group of Ser92. This conserved hydrogen-bonding network may affect the ligand-binding barrier by fixing the position of the His93 imidazole ring or hindering its rotation. A projection of the plane of the His93 imidazole ring onto the heme plane is nearly coincident with the axis of the heme group formed by the pyrrole N_2 and N_4 atoms and the central iron. In the WT deoxy and met proteins this projection lies at an angle of 19° rotated clockwise from the N_2-Fe-N_4 axis when viewed from the proximal side (*19, 24, 25*). This nearly "eclipsed configuration" appears to be sterically unfavorable due to the close proximity of these pyrrole nitrogens with the C_δ and C_ϵ of the imidazole ring (∼3.1 Å). This steric hindrance could be relieved by movement of the iron out of plane, as occurs in the deoxy state, or by rotation of the imidazole ring relative to the heme pyrrole nitrogens. Thus, at least part of the barrier to ligand binding must involve the energy required to pull the iron back into the heme plane against these steric interactions on the proximal side.

Smerdon et al. (*26*) have characterized three proximal mutants in pig myoglobin in which Ser92 is replaced with alanine, valine (the residue in lupin leghemoglobin (*27, 28*)), or leucine (the residue in human HbA). All three of these mutations eliminate the hydrogen bonds from position 92 to both His93 and the 7-propionate. These mutations result in an increase in the overall affinity of the protein for CO, O_2, and substituted isocyanides with the order of the effect increasing as Ala < Val ≤ Leu. Heme dissociation was also found to increase. The 2.7 Å X-ray structure for the aquomet derivative of the Leu mutant indicated that the position of the Leu side chain is disordered and is in a geometry pointing away from the His93 imidazole. In addition, the 7-propionate was found to be disordered and no longer H-bonded to His97. The His97 side chain was rotated, and solvent accessibility to the proximal side of the heme pocket had increased. Surprisingly, no rotation of the His93 imidazole

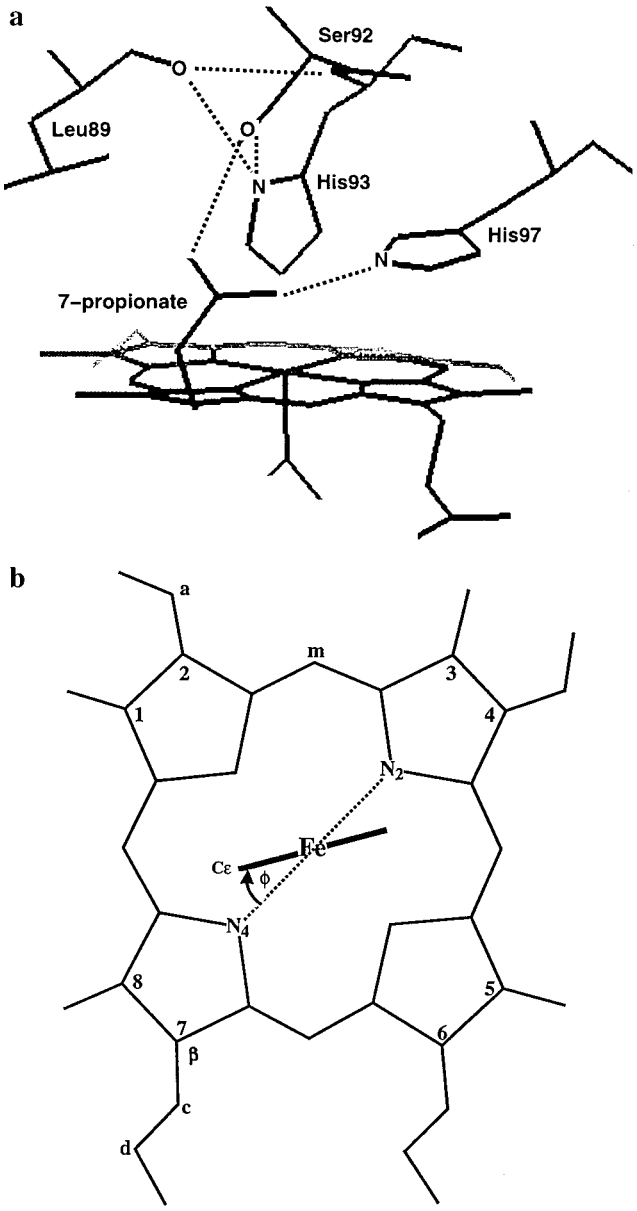

FIGURE 1: (a) Proximal heme pocket showing the hydrogen bonds between the $N_\delta H$ of the His93 imidazole ring and the hydroxyl side chain of Ser92 and the carbonyl of Leu89. Also shown are the hydrogen bonds from the 7-propionate carboxylate group to the hydroxyl of Ser92 and the imidazole of His97. (b) Proximal view of the heme showing the numbering scheme used to label the Raman modes and the azimuthal angle, ϕ (using the same sign convention as in Yamamoto et al. (*24*)). The His93 azimuthal angles reported herein were measured as the dihedral angle about the proximal His−Fe bond between the imidazole $N_\epsilon-C_\epsilon$ and heme $Fe-N_4$ bonds.

[1] Abbreviations: Mb, myoglobin; swMb, sperm whale Mb; Hb, hemoglobin; HbA, human hemoglobin A; HbI, dimeric hemoglobin from the blood clam Scapharca inaequivalvis; Mb*, photoproduct of carbonmonoxy Mb at 10 ns; L89I, mutant swMb Leu89 → Ile; H97F, mutant swMb His97 → Phe; S92A, mutant swMb Ser92 → Ala; S92P, mutant swMb Ser92 → Pro; F-swap, mutant swMb with swMb residues 87−94 (Lys-Pro-Leu-Ala-Gln-Ser-His-Ala) replaced with HbA β chain residues 86−93 (Ala-Thr-Leu-Ser-Glu-Leu-His-Cys); fwhm, full width at half-maximum intensity.

ring was observed, but it is possible that the resolution of the structure was inadequate for this to be seen had it occurred.

Shiro et al. (*29*) have further characterized the Ser92Ala mutant, but in human myoglobin. Their NMR data indicate that the distal pocket is unchanged, that the His97 side chain has moved, but not as much as Smerdon et al. report, and that the azimuthal angle of the His93 imidazole ring in the cyanomet form has increased via a rotation of ~5° toward the Leu89 carbonyl group. (Note: Shiro et al. reference Yamamoto et al. (*24*) for the azimuthal angle angular convention, but in their text they have it reversed. Yamamoto's convention is a clockwise rotation (larger values of ϕ) when viewed from the *proximal* side as described above and shown in Figure 1b.) The CO and O_2 on and off rates in the Ala mutant were found to be essentially unaffected by the mutation at position 92. Visible Raman spectra revealed a 3 cm^{-1} increase in the ν(Fe−His) band associated with the proximal bond between the iron and the His93 side chain, indicating that this bond is slightly stronger in the Ser92Ala mutant.

Lloyd et al. (*30*) have characterized the Ser92Asp mutant in horse heart myoglobin. X-ray data on the met form from this study revealed that the Asp92 side chain was disordered and that a best fit to the electron density positioned the chain pointing out of the proximal pocket away from His93, as was the case with the Leu side chain studied by Smerdon et al. (*26*). The position of the His93 imidazole ring, the Fe−His bond length (2.1 Å), and the hydrogen-bond length to the Leu89 carbonyl (3.1 Å) were unchanged from the values in the WT protein within the accuracy of the structure. The position of the 7-propionate was shifted 0.63 Å out of the heme pocket, but the hydrogen bond to His97 was maintained. NMR measurements on the cyanomet derivative indicate that the His93 imidazole has rotated about 5° toward the Leu89 carbonyl thus adopting a less eclipsed geometry, the same result that Shiro et al. found with the Ala92 mutation. The NMR data on the met, cyanomet, and deoxy proteins also revealed a titratable transition with a pK_a of ~6 involving protons in the region of the 7-propionate group. This was assigned to the protonation of the His97 side chain, but it is unclear if it was this side chain or the 7-propionic acid carboxylate group that was being protonated. Raman data on the cyanomet derivative show no changes in the bands from 400 to 1700 cm^{-1}, but the propionate-sensitive bands from 250 to 400 cm^{-1} have broadened or split into additional bands indicating that this mutation has introduced some degree of disorder within the heme pocket.

Sinclair et al. (*31*) have performed X-ray absorption spectroscopy on the met forms of WT, Leu89Ile, Leu89Val, and Leu89Asp sperm whale myoglobins. They calculated the Fe−His bond length in these proteins to be 2.14, 2.13, 2.28, and 1.91 Å, respectively. The Debye−Waller factors from the EXAFS structure determination indicate that the Leu89Val and Leu89Ile mutants have increased disorder in the Fe−His bond, while the Leu89Asp has the least disorder. In the Val and Ile mutants these observations were attributed to a possible lack of a hydrogen bond to the His93 imidazole from the 89 carbonyl and also to the smaller size or shape change of these side chains, both of which would allow more freedom of movement or volume for the His93 imidazole. The increased order in the Asp mutant was attributed to an increased hydrogen-bond strength to the His93 imidazole via a backbone chain rotation in which the hydrogen bonds to the Ser92 hydroxyl and the 89 carbonyl have been replaced with a hydrogen bond to the Asp carboxylate. A shortening of the Fe−His bond in the Asp mutant would then follow due to increased electron density in the Fe−His93-heme system. However, rotation of the His93 imidazole could also allow the Fe−His bond to shorten due to reduction of the steric interference between the imidazole carbons and the pyrrole nitrogens of the heme.

In all of the studies done thus far on the hydrogen-bonding network in Mb, only one mutation has been made at a time, and in most cases large deviations from wild-type behavior are not seen in these mutants. Thus, it is not clear from these studies if the proximal hydrogen-bonding network is crucial in maintaining a wild-type geometry or if other factors, such as the covalent bond to the F-helix and/or steric packing forces, maintain the geometry that produces the ligand-binding behavior seen in wild-type Mb. Toward the goal of a more complete understanding of the role of this highly conserved proximal hydrogen-bond network, we have used site-directed mutagenesis to produce several mutants of sperm whale myoglobin (swMb) that alter or eliminate one or more of these hydrogen bonds. Leu89Ile (L89I) was made as a small perturbation of the network. This mutation should only produce a change in the steric factors of the pocket as it involves only a shift of a methyl group and should not change the electrostatic environment or result in the removal of a hydrogen bond. His97Phe (H97F) eliminates one H-bond to the heme 7-propionate group, but maintains the presence of an aromatic ring in close proximity to the porphyrin macrocycle. Ser92Ala (S92A) and Ser92Pro (S92P) both eliminate the H-bonds to the His93 $N_\delta H$ and one of the bonds to the 7-propionate group. The Ala group is small and unpolar, while the Pro group, known to disrupt an α helix, should produce a large change in the local geometry of the F-helix and probably of the His93 imidazole ring as well. The His97Phe-Ser92Ala (H97F-S92A) and His97Phe-Ser92Pro (H97F-S92P) combine the effects of the single mutations and eliminate all the H-bonds except the one to the backbone carbonyl of Leu89. Finally, as a potentially large change of the proximal environment, an F-swap mutant was constructed in which eight amino acids from the β subunit of human hemoglobin, HbA, were substituted for the corresponding residues in swMb: swMb residues 87−94, Lys-Pro-**Leu**-Ala-Gln-**Ser**-*His*-Ala → β chain 86−93 Ala-Thr-**Leu**-Ser-Glu-**Leu**-*His*-Cys. The residues at the key positions 89 and 92 that are normally involved in the swMb H-bond network are marked in bold and underlined, and the proximal His is italicized. Note that this mutation leaves the swMb His97 and Leu89 intact, so the most readily apparent change is the elimination of Ser92 and its associated H-bonds. The rationale behind this seemingly drastic mutation is that the structure of Mb most closely resembles the isolated β chain of HbA; both the α chain and the intact HbA tetramer display greater differences. A detailed comparison between the isolated α and β chains, swMb, the F-swap mutant, and HbA will be published elsewhere, as will the bimolecular ligand-binding kinetics and the NMR structures of the heme pockets (*32*). In this work we report Resonance Raman data on the deoxy and CO photoproduct at 10 ns, CO geminate recombination

kinetics, and molecular modeling of the CO state to characterize these proximal mutants. Ramifications of changes in the proximal hydrogen-bonding network in myoglobin are discussed.

MATERIALS AND METHODS

Site-Directed Mutagenesis. Single or double mutations of sperm whale myoglobin at positions 89, 92, and 97 as well as an F-swap mutant in which residues 87−94 of the myoglobin F-helix were replaced with residues 86−93 from the F-helix in the β subunit of human hemoglobin HbA were generated using the cassette mutagenesis technique following procedures described in detail elsewhere (*12*, *33*, *34*). Briefly, oligonucleotides were synthesized by the University of Illinois Biotechnology Center. Typically, 400 pmol of oligonucleotides was phosphorylated with ATP and T4 polynucleotide kinase. The cassette was generated by slowly annealing 100 pmol of oligonucleotide in 10 μL of water. The cassette was ligated into plasmid DNA (pMb122) which had been digested with the appropriate restriction enzyme, and then transformed into *Escherichia coli* TB-1 cells with the exception that the ligated plasmid for the F-swap mutant was transformed into *E. coli* strain BL21(DE3) instead of TB-1. The sequence error incorporating asparagine at position 122 was corrected to the wild-type aspartic acid.

Protein Expression and Purification. With the exception of the F-swap mutant, all of the Mb mutants were purified as described in Abadan et al. (*33*) and equilibrated in 0.1 M sodium phosphate buffer at 7.4 in the met form and 1−3 mM in concentration. For the F-swap mutant, the plasmid was extracted from BL21(DE3) and transformed into *E. coli* TB-1 for expression of the mutant. The protein was purified using the same procedure described in Springer and Sligar (*35*) with the following modifications. Following the 60%−90% ammonium sulfate salt cut, the pellet was resuspended in a minimum amount of 50 mM sodium phosphate buffer, pH 7.0, and dialyzed overnight against water to remove all of the ammonium sulfate in solution. The pH of the protein solution was lowered to 6.0 with NaH_2PO_4 and loaded onto a CM-52 column (Whatman, Inc., Fairfield, NJ) that was equilibrated with 10 mM sodium phosphate, pH 6.0. The protein was eluted from the column with 0.1 M sodium phosphate, pH 7.0. The eluent from the CM-52 column was concentrated, loaded onto a Sephadex G-25 column (Pharmacia Biotech, Piscataway, NJ) equilibrated with 0.1 M sodium phosphate, pH 7.5, and eluted with the same buffer. Appropriate fractions from the column were pooled, concentrated, and stored at −70 °C until used.

Raman Sample Preparation and Apparatus. The sample preparation and the experimental apparatus for the Raman experiments have been described in detail elsewhere (*47*). Briefly, all of the samples were approximately 1 mM in heme and in pH 7.4, 0.1 M phosphate buffer. CO derivatives were prepared from concentrated met stock solutions diluted with buffer by passing CO gas over the surface of a 100 μL aliquot in a sealed vial sample and then adding approximately 5 equiv with respect to the heme concentration of sodium dithionite. Deoxy derivatives were prepared in same manner but with N_2 gas instead of CO. The sample cell was cooled to approximately 10 °C and rotated fast enough such that a new sample volume was interrogated with each laser shot. Photoproduct buildup and artifacts from sample spinning were found to be negligible by varying the spinning rate and by taking visible absorption spectra before and after each experiment.

Visible time-resolved resonance Raman spectra were obtained using an 8 ns, 150 μJ, 435.8 nm pulse to both photodissociate the ligand and Raman scatter off the sample. The laser used was a frequency-doubled Nd:YAG laser (Continuum NY81C-20, Santa Clara, CA) that was frequency-shifted via stimulated Raman scattering in a hydrogen cell. The detector was an intensified diode array run in the cw mode (Princeton Instruments P/N IRY-1024S/B, Trenton, NJ). The spectral bandwidth of the monochromator was approximately 2.5 cm^{-1}, and the resolution of the detector array was approximately 0.9 cm^{-1}/pixel.

Raman Spectra Data Processing and Fitting. Raman spectra were calibrated using solvent spectra with previously determined peak assignments. A least-squares fit was used to map the pixel number into relative wavenumbers (Raman shift). The Raman spectra were baselined using a polynomial fitting routine in LabCalc (Galactic Industries, Salem, NH), were normalized in intensity using the ν_7 mode band at ∼672 cm^{-1}, and are presented without smoothing.

The ν(Fe−His) band in the Raman spectra of the CO photoproduct at 10 ns was fit to a sum of Lorentzian functions using GRAMS software (Galactic Industries, Salem, NH). The spectra were initially fit to two or three Lorentzians in which the amplitudes, widths, and center frequencies were allowed to vary. This was found to be inadequate for at least two reasons. First, some of the mutant spectra had ν(Fe−His) bands that had edges that were too steep to be accommodated by only two or three Lorentzians if they were also to be wide enough to span the total band. Second, it was impossible to get the three-Lorentzian fit in which all three variables for each component were allowed to float to converge on a unique solution. We attempted to help this convergence by fixing the widths and then the frequencies in an alternating fashion, but this did not provide sufficient control to drive the fit into a unique solution. To attain a unique fit we fixed the widths of the Lorentzians. It is not possible from the data presented herein to ascertain the distribution of conformational subpopulations or the ν(Fe−His) line widths associated with their individual spectra. The heme modes in the Raman spectra are typically 13−16 cm^{-1} fwhm, so a width of this magnitude was chosen as an estimate of the width of each subpopulation's ν(Fe−His) line shape. A minimum of four Lorentzians of this width is required to fill the total profile of the ν(Fe−His) band. The ν(Fe−His) band can, of course, be fit to more components, but a unique fit becomes difficult to achieve if more than five or six Lorentzians of this width are used. For the purposes herein, fitting with four Lorentzians was sufficient to describe the differences in the mutant Raman spectra. To determine the sensitivity of the fit to a given line width, we fit the ν(Fe−His) band in the CO photoproduct Raman data to a set of four Lorentzians with a fwhm of 14 cm^{-1} and then repeated the process using a width of 16 cm^{-1}. The results for both of these widths exhibited the same trends in the resulting fitting parameters. The reduced χ^2 values for all the fits with the 16 cm^{-1} Lorentzians were between 1.5 and 2.5. The values for reduced χ^2 are more of an internal standard by which to gauge the goodness of fit,

however, rather than a rigorous statistical measure, since it is not clear what value to use for the standard deviation of the noise. The signal-to-noise in the RR spectra is not limited by photon shot noise but rather is limited by the pixel-to-pixel variation in the gain of the intensifier coating on the diode array. This noise is not likely to follow a Normal (Gaussian) distribution. Furthermore the pixel-to-pixel variation is neither consistent throughout the array nor constant at any given point in the array. Since the pixel-to-pixel variation depends on what area of the diode is illuminated as well as the intensity of the light, it is not possible to completely subtract the "noise" generated by this effect from the spectra by doing a flat field separation. For the purposes of estimating the noise value for the reduced χ^2 calculation, the noise was estimated using several regions of the spectrum that were free from Raman peaks. The same regions were used in each spectrum for the sake of consistency.

Flash Photolysis Sample Preparation. A sample cuvette was stoppered with a septum and purged with N_2 or Ar. Concentrated protein stock solution was transferred to the cuvette and diluted with deoxygenated buffer to a final protein concentration of 5 μM. Dithionite was added to reduce the iron, and the UV/vis absorbance spectrum was taken to ensure that full reduction had taken place and that the sample was fully deoxygenated. CO was then added to the sample. The sample temperature was maintained at 20 °C for the geminate-rebinding measurements.

Flash Photolysis Apparatus. The nanosecond flash photolysis apparatus is described in detail elsewhere (*36*). Briefly, a 10 ns 532 nm pulse from a Nd:YAG laser (Spectra Physics GCR150, Mountain View, CA) was used to photolyze the CO−iron bond in the MbCO, and the CO recombination kinetics were monitored by absorption changes in the Soret spectral region at 420 nm (bound state recovery) or 435 nm (photolyzed state decay) using a Xe arc lamp (Cermax 500W, ILC Technology, Sunnyvale, CA) as the probe source. The probe beam was passed through a monochromator for wavelength selection and isolation from the 532 nm photolysis light, and the time-dependent intensity was measured with a PMT. The PMT signal was amplified (Stanford Research SRS560 low noise preamp) and then digitized and stored in an oscilloscope (Model 9350, LeCroy Corp., Chestnut Ridge, NY). Data traces from 50 to 150 laser pulses were averaged to obtain sufficient signal-to-noise values for analysis. The raw transmission data were converted to transient change in absorbance by taking the logarithm and using the segment of data prior to the 532 nm photolysis pulse as the baseline. The data were curvefit using the function $A(t) = A_0 + A_1\exp(-k_{obs}t)$.

Molecular Modeling. The appropriate amino acids were replaced in the WT MbCO structure (*20*), using QUANTA (Molecular Simulations, Inc., San Diego, CA), and the resulting structure was energy-minimized using CHARMM (Molecular Simulations, Inc., San Diego, CA). The His93 azimuthal rotation angle was measured as the dihedral angle about the proximal His−Fe bond between the $N_\epsilon-C_\epsilon$ bond in the His93 imidazole plane and the heme $Fe-N_4$ bond (Figure 1b). Note, this method of measurement will give slightly different angular values than the projection of the imidazole plane into the heme plane as used by Yamamoto et al. (*24*), but changes in the azimuthal angle due to mutation can be monitored either way equally well.

RESULTS

Raman. The Raman spectra from 150 to 900 cm^{-1} of the CO photoproduct at 10 ns (Mb*) of the WT and mutant proteins are shown in Figure 2, and comparison of the low-frequency region with the corresponding spectra of the deoxy derivatives is shown in Figure 3. The spectra in Figures 2 and 3 were normalized[2] using the ν_7 band at ~672 cm^{-1}. The choice of ν_7 was based upon the insensitivity of this band to the proximal mutations as verified by the excellent overlap of several mid- and high-frequency bands in the spectrum after this normalization. Essentially all of the differences due to either the mutations or the change in ligation state of the heme are present in the lower-frequency region of the spectrum between 180 and 400 cm^{-1}. An enlarged view of this region is displayed in Figure 3 and contains the following peak assignments (*37, 38*). The large, broad peak at ~220 cm^{-1} is ν(Fe−His) and is due to the stretching mode of the proximal bond between the heme iron and the N_ϵ of His93. The shoulder on the high-frequency side of the ν(Fe−His) band has been assigned to ν_9, a pyrrole tilting mode (*38*−*40*). The peak at ~300 cm^{-1} is γ_7, assigned to an out-of-plane methine wag mode involving C_a and C_m. The peak at ~335 cm^{-1} is γ_6, a pyrrole tilting mode. The peak at ~342 cm^{-1} is ν_8, assigned to a pyrrole stretch and substituent bending mode. The peak at 364−371 cm^{-1} is assigned to $\delta(C_\beta C_c C_d)$, a mode involving bending of the propionate methylene groups. The spin state and heme core size marker bands in the high-frequency region, 1350−1600 cm^{-1}, do display the expected changes for the transition from the deoxy, five-coordinate, spin = 2 heme to the ligated, six-coordinate, spin = 0 heme (data not shown).

ν(Fe−His) Mode. The positions of maximum intensity of the ν(Fe−His) mode peaks for the CO photoproduct and deoxy spectra are tabulated in Table 1. The frequency difference between these two derivatives is also tabulated. The wild-type protein displays the largest frequency difference and the L89I, S92A, and F-swap proteins have a slight reduction in this shift. The H97F and H97F−S92A proteins show the smallest difference.

The changes due to the mutations in the ν(Fe−His) band profile of the CO photoproduct were studied in more detail via a curve-fitting analysis. The results of a curve fit to four Lorentzian peaks with a fixed width of 16 cm^{-1} fwhm are shown in Table 2. When comparing the changes in the components of the fit, one must keep in mind that an apparent shift or change in the intensity of one edge of the Raman band can be achieved in one of two ways: through either a frequency shift of the component peak at that edge or a

[2] The importance of such normalization in determining all of the changes in the bands due to the mutations is illustrated with a simple example. Consider the simplified case in which the WT band is composed of two subcomponents of equal amplitude and the mutant band is reduced in intensity such that component 1 is decreased to $^1/_3$ of that seen in the WT and component 2 is reduced to $^2/_3$ of the WT value. If the two bands were merely overlapped by matching their intensities, it would appear that component 1 had decreased to half of its WT value and that component 2 had remained the same. Thus, without an "external" standard, the change in the ratio of the two component intensities is discernible (a change from the WT value of 1:1 to the mutant value of 1:2), but the fact that both components actually decrease in amplitude in the mutant spectrum is missed.

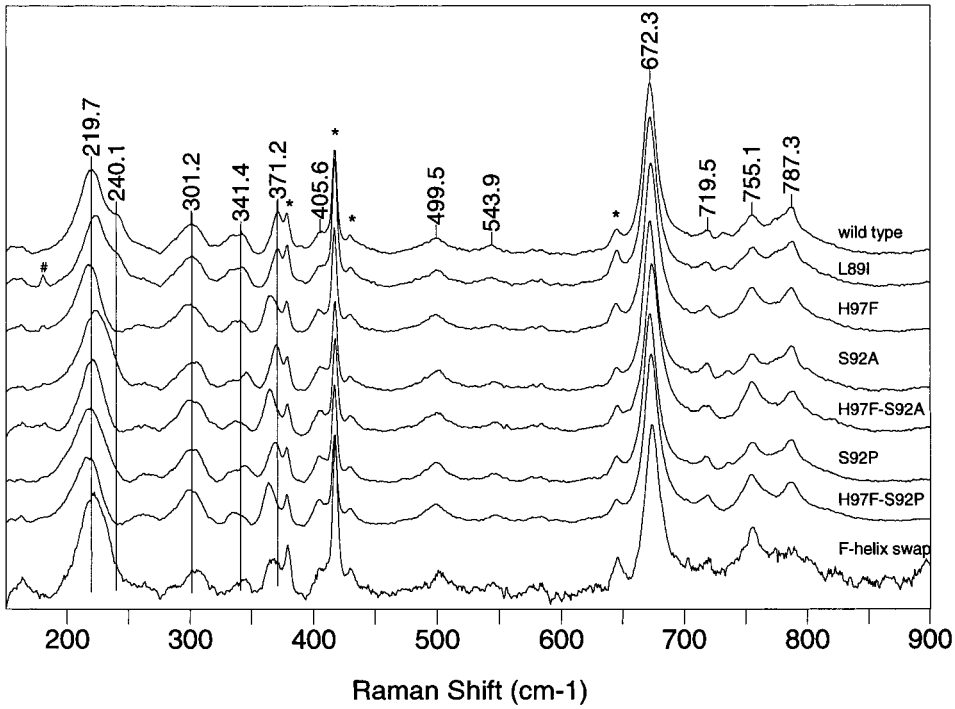

FIGURE 2: Visible resonance-enhanced Raman spectra from 150 to 900 cm^{-1} of the CO photoproduct at 10 ns (Mb*) of the WT and proximal mutant swMb's. Laser wavelength = 435.8 nm and power = ~3 mW. All samples were in 0.10 M phosphate buffer, pH 7.4. Spectra were normalized to the ν_7 mode at ~672 cm^{-1}. The peaks marked with an * are due to Raman scattering from the sapphire window used on the front of the optical cell, and the peaks marked with a # are from a laser line from Raman shifting off rotationally hot H_2 in the hydrogen cell used to create the 435.8 nm beam in the laser system. Other experimental details are as in the Methods section.

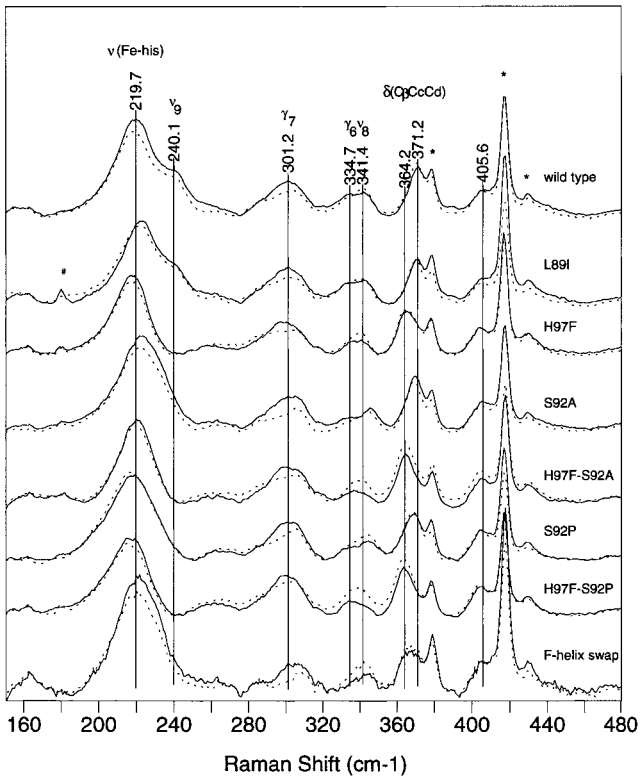

FIGURE 3: Enlarged view of the low-frequency region of the visible resonance-enhanced Raman spectra from 150 to 480 cm^{-1} of the CO photoproduct at 10 ns (solid line) and deoxy derivatives (dotted line) of the WT and proximal mutant swMb's. Details are as in Figure 2 and in the Methods section.

change in its amplitude relative to the other components. If both of these occur in a compensatory manner, as in the highest-frequency component in the S92P fit, only a small shift or change may be evident in the sum curve. To check to see that the changes revealed in the curve fitting are actually present in the data, the individual curves were overlapped, examples of which are shown in Figure 4. All of the mutations except the F-swap resulted in a decrease in the ν(Fe−His) band intensity, so the spectra in Figure 4 were normalized to the same ν(Fe−His) intensity to clearly show the changes in band profile. It should be noted that the fitting results listed in Table 2 indicate the relative areas of the four components within the ν(Fe−His)−ν_9 band envelope of a given protein and therefore indicate changes of line shape, but these relative areas are not normalized across all of the proteins and so cannot be used to ascertain how the overall band intensity varies from protein to protein, as discussed above in the footnote example. The normalized curves themselves, as shown in Figure 3, should be used for this purpose. Representative examples of the curve fitting are shown in Figure 5.

The ν(Fe−His) band profiles of the WT and L89I peaks are very nearly identical, but the L89I peak is shifted up in frequency and is slightly less intense. In fact, if the L89I data is shifted down by ~3 cm^{-1} and multiplied by a scalar it overlaps the WT spectra almost exactly within the signal-to-noise. The curve-fitting results are consistent with this shift. All of the other mutants display dramatic changes in the ν(Fe−His) band profile. The H97F mutant shows a decrease in the frequency of the highest-frequency component, essentially no change in the low-frequency edge (note that this is represented by two bands in the fit since there is no ν_9 band), and a disappearance of the ν_9, or "240", band. The S92A and the F-swap mutants show a shift in the population to the high-frequency components and a decrease in the frequency of the ν_9 band. The S92P mutant line shape

Table 1: Low-Frequency Raman Band Frequencies, Geminate Recombination Parameters, and His93 Azimuthal Angle

	ν(Fe-His)[a]							
protein	Mb*CO	deoxy	difference	$\delta(C_\beta C_c C_d)$[a]	$\nu_9 = 240$ band[a]	k_{obs} GR $\times 10^{-7}$ (s^{-1})	GR yield (%)	azim. angle, ϕ[b]
WT	219.7	218.4	1.3	371.2	240.1	1.44 ± 0.42	4.6 ± 0.8	10.3
L89I	222.7	221.7	1.0	370.8	240.0	1.40 ± 0.23	5.9 ± 1.0	12.2
H97F	217.9	217.6	0.3	365.6		2.02 ± 1.40	6.1 ± 0.2	5.2
S92A	222.8	221.7	1.1	369.9	232.9	1.65 ± 0.15	7.4 ± 0.7	16.4
H97F-S92A	219.5	219.0	0.5	364.5		1.98 ± 0.60	4.3 ± 0.7	15.0
S92P	218.1	217.3	0.8	369.2	229.2[c]	2.19 ± 0.92	3.1 ± 0.6	3.0
H97F-S92P	217.1	216.2	0.9	364.2		2.85 ± 0.64	4.8 ± 0.8	1.5
F-swap	220.5	219.4	1.1	366.7	230.8	1.2 ± 0.22	15 ± 1.7	19

[a] frequency at maximum band intensity. [b] Dihedral angle between the Fe−N_4 heme bond and the His 93 imidazole N_ϵ−C_ϵ bond. [c] It is unclear if this component is a very low-frequency ν_9 band or the high-frequency edge of ν(Fe-His).

Table 2: Results of Curve Fitting the ν(Fe-His)−ν_9 Composite Band Profile to Four Lorentzian Lineshapes with the Width, fwhm, Fixed at 16 cm^{-1} and with Unconstrained Frequencies and Amplitudes[a]

protein	ω	area (%)	ω	area (%)	ω	area (%)	ω	area (%)	ω	area (%)	ω	area (%)
WT			205.5	9	215.9	38	223.6	35			240.1	18
L89I			210.7	10	219.4	34	225.5	39			240.0	18
H97F	194.4	5	207.4	14	215.2	38	221.7	44				
S92A			204.3	8	215.8	27	223.9	41	232.9	25		
H97F-S92A			207.5	10	216.2	37	222.0	37	226.7	16		
S92P			198.7	12	210.9	27	219.8	41	229.2	22		
H97F-S92P	192.4	4	203.7	16	213.8	39	221.9	41				
F-swap			201.8	8	213.7	26	221.8	42	230.8	26		

[a] The table shows center frequency in wavenumbers of each component and the area percentage of that component relative to the total area under the composite band profile. Estimated errors: frequencies, $\pm$ 0.2 cm^{-1}; areas, $\pm$ 2%.

shows a relative increase in intensity on the low-frequency edge, while the high-frequency edge is similar to the WT but is lacking the ν_9 band. It is noteworthy that the three proteins involving a mutation at position 92, but not at 97, exhibit the same band profiles and differ primarily through shifts of a few wavenumbers of the entire band such that the peak frequencies increase in the order S92P (218.1 cm^{-1}) < F-swap (220.5 cm^{-1}) < S92A (222.8 cm^{-1}). This same progression is seen in the components in the curvefits to these spectra (Table 2). The ν(Fe−His) band profiles of the two double mutants, H97F−S92A and H97F−S92P, indicate that the two mutations are independently affecting the protein structure, that is, their combined effects are additive. For example, the H97F−S92A band is narrow like that of H97F due to the loss of the high-frequency edge, but the whole profile is shifted up in frequency as in S92A.

These differences in the ν(Fe−His) portion of the band in the mutant spectra with respect to the WT are apparent in the results of the curve-fitting analysis as changes in the relative populations of components with the same frequencies as the WT (as in S92A), as an equivalent shift in the frequencies of all the components but maintaining population ratios close to those seen in WT (as in L89I), or as a combination of changes in both frequencies and relative populations (as in H97F and the double mutants).

γ_7. The γ_7 mode is sensitive to disorder in the heme pocket (*37, 38*). The appearance of this band in the mutant spectra is largely unchanged in comparison to the wild type, although there are small shifts in frequency that correlate somewhat with the shifts in the ν(Fe−His) band position. The CO spectra display a broad feature centered at ~300 cm^{-1}, while in the deoxy spectra this peak is decreased in intensity and is split into a main band at ~303 cm^{-1} with a shoulder at ~290 cm^{-1}. The F-swap deoxy spectrum shows a very clear split between these two components.

Propionate-Sensitive Modes: γ_6, ν_8, ν_9, and $\delta(C_\beta C_c C_d)$. These modes involve out-of-plane motions of the heme and bending motions of the peripheral groups and appear in the low-frequency region of the Raman spectrum (Figure 3 and Table 1). In the WT and L89I Mb* spectra the γ_6 band at 335 cm^{-1} and the ν_8 band at 342 cm^{-1} are well separated and are of comparable intensity. In the S92A and S92P Mb* spectra, ν_8 has shifted up to ~ 345 cm^{-1}. In the H97F, H97F−S92A, and H97F−S92P Mb* spectra, the frequency difference between the γ_6 and ν_8 bands has decreased so that they have coalesced into a single asymmetric band centered at ~340 cm^{-1}. The F-swap mutant displays an intensity decrease in both bands, but more so in the γ_6 band. The deoxy spectra display the same trends as in the Mb* spectra but with slightly increased intensity in both bands.

The ν_9 (240 band) and $\delta(C_\beta C_c C_d)$ bands undergo some of the most interesting changes in these spectra. The behavior of the Mb* and deoxy states are the same. A strong correlation is apparent between the position of the ν_9 band and that of the $\delta(C_\beta C_c C_d)$ band. Whenever the $\delta(C_\beta C_c C_d)$ band is above ~370 cm^{-1}, the ν_9 band appears as a shoulder on the ν(Fe−His) profile at 240 cm^{-1}. If the $\delta(C_\beta C_c C_d)$ appears at a lower frequency, then ν_9 either blends smoothly into the ν(Fe−His) envelope or is apparently missing altogether. The ν_9 band was included in the curve-fitting analysis of ν(Fe−His), and the results are tabulated in Tables 1 and 2. Table 1 also includes the position of the $\delta(C_\beta C_c C_d)$ band.

Both the WT and the L89I spectra have a prominent ν_9 band at 240 cm^{-1} and a $\delta(C_\beta C_c C_d)$ band at 371 cm^{-1}. In the S92A and the F-swap mutant spectra, ν_9 is at ~232 cm^{-1} and the $\delta(C_\beta C_c C_d)$ band is at 370 and 367 cm^{-1}, respectively. In the H97F, H97F−S92A, and H97F−S92P spectra ν_9 seems to have disappeared completely and the $\delta(C_\beta C_c C_d)$ band is at ~365 cm^{-1}. In the S92P spectrum it is difficult

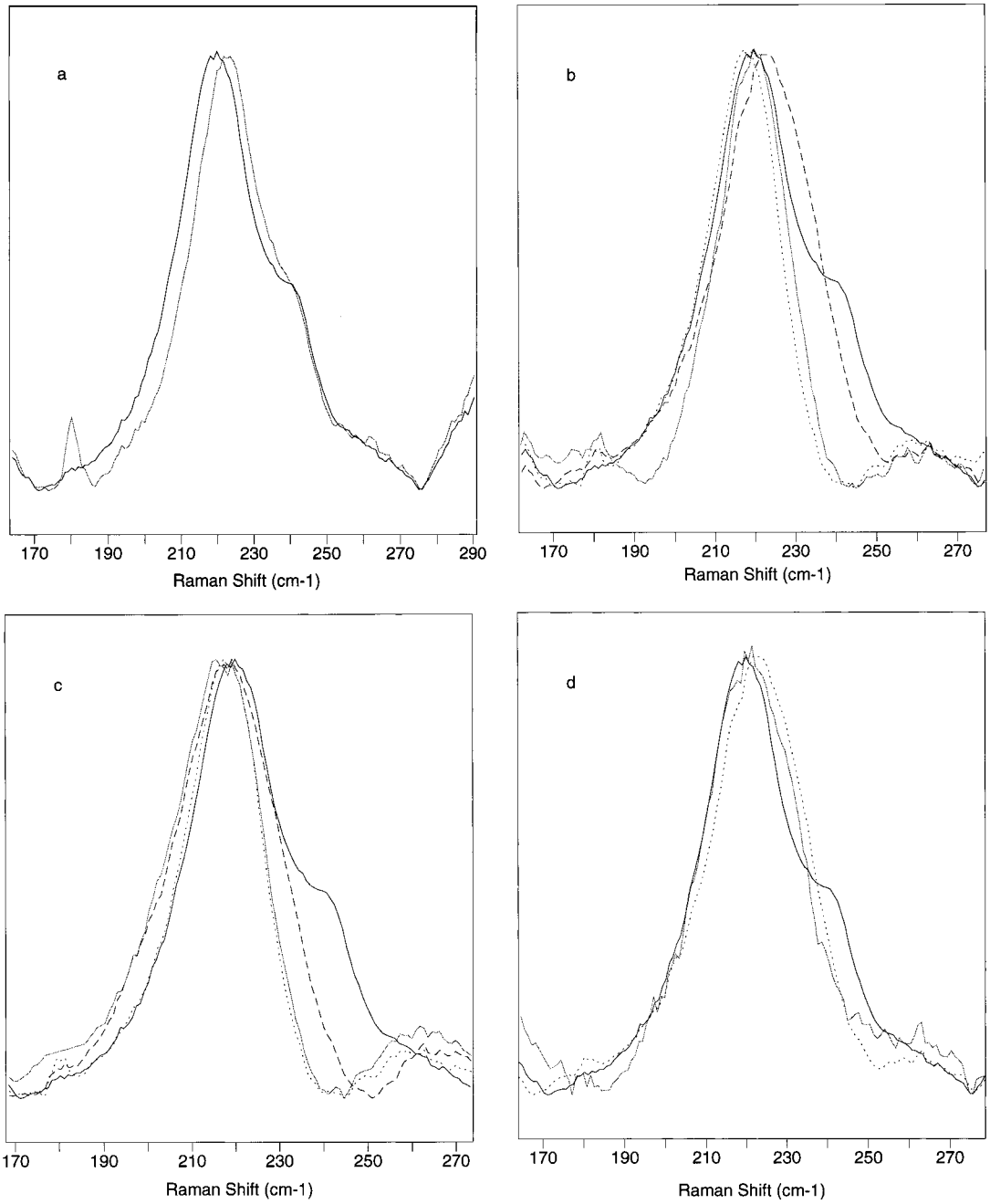

FIGURE 4: Overlap of the ν(Fe−His) bands of the WT and mutants from the spectra of the CO photoproduct at 10 ns shown in Figure 2 demonstrating the changes in profile. These spectra were normalized to the ν(Fe−His) intensity, not the ν_7 intensity. Hence, the differences shown here only show changes in the population distribution among the different frequency components of the band and not overall changes in the band intensity: (a) WT (solid line) and L89I (gray line); (b) WT (solid line), H97F (dotted line), S92A (dashed line), and H97F−S92A (gray line); (c) WT (solid line), H97F (dotted line), S92P (dashed line), and H97F−S92P (gray line); (d) WT (solid line), S92A (dotted line), and F-swap (gray line).

to ascertain if the highest-frequency component at 229 cm^{-1} is part of ν(Fe−His) or just a very low-frequency ν_9 band and the $\delta(C_\beta C_c C_d)$ band appears at 369 cm^{-1}. As was the case in the ν(Fe−His) band, the $\delta(C_\beta C_c C_d)$ band in the double mutants exhibits behavior as if the perturbations of the individual mutations are additive: the frequency shift of this band in the double mutants is approximately the sum of that seen in the single mutants.

pH Dependence of Wild Type and His97Phe. The Mb* RR spectra for the WT and H97F proteins were collected at pH 5.1, 6.2, and 7.4 and are shown in Figure 6. There are not any large pH-dependent changes throughout the spectra from 150 to 900 cm^{-1}. However, in the WT spectrum at pH 5.1, there are small intensity changes in γ_7, ν_8, and $\delta(C_\beta C_c C_d)$, and there is less overlap of γ_6 at 333 cm^{-1} and ν_8 at 344 cm^{-1}. Inexplicably, the WT ν(Fe−His)−ν_9 band envelope is more intense at pH 6.2 than at either pH 7.4 or 5.1. In the H97F spectra, the $\delta(C_\beta C_c C_d)$ band shifts up in frequency from 366 cm^{-1} at pH 7.4 to 368 cm^{-1} at pH 5.1 and there are small changes in the overlap of γ_6 and ν_8.

Geminate Recombination Kinetics and Yields. The geminate recombination rates and yields are tabulated in Table 1. The rates are the observed rates and have not been separated into the true geminate-rebinding rate and rate of escape from the pocket. From the values determined for k_{obs} it can be seen that the geminate kinetics are essentially

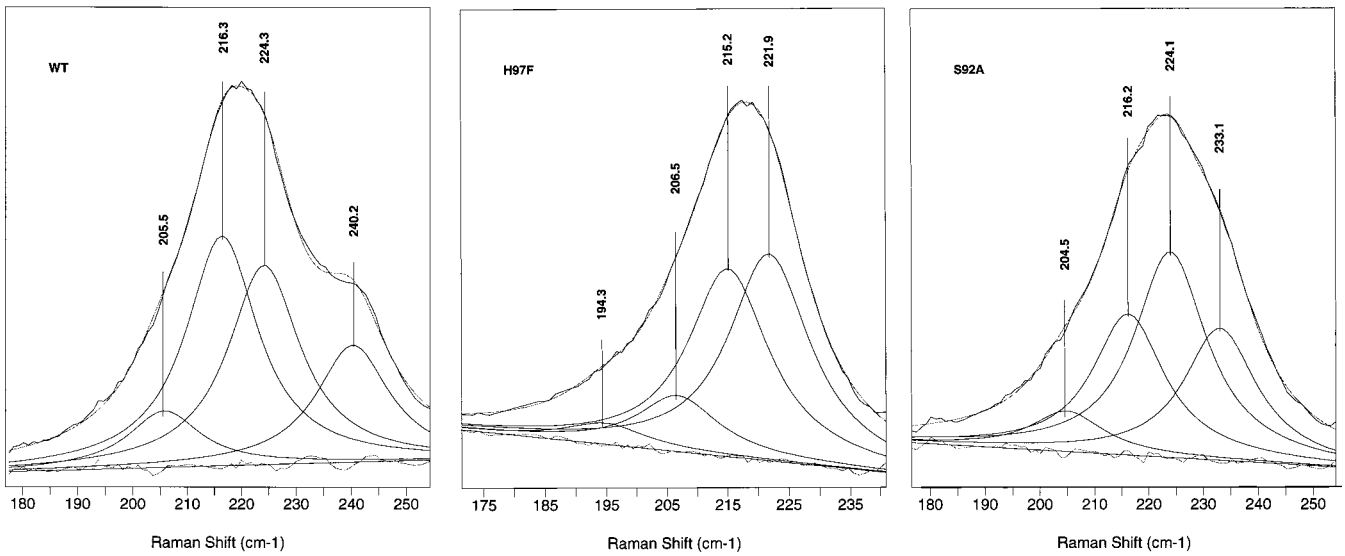

FIGURE 5: Examples of curve fitting to the ν(Fe−His) bands of the WT, H97F, and S92A 10 ns CO photoproduct spectra as shown in Figure 2. The individual components are Lorentzian line shapes with a fwhm of 16 cm^{-1}. The data, baseline, and subcomponent lines are depicted as solid curves, while the fit sum and residuals are shown as gray curves. The peak frequencies shown differ slightly from those in Table 2 since the table values are averages of fits to several data curves.

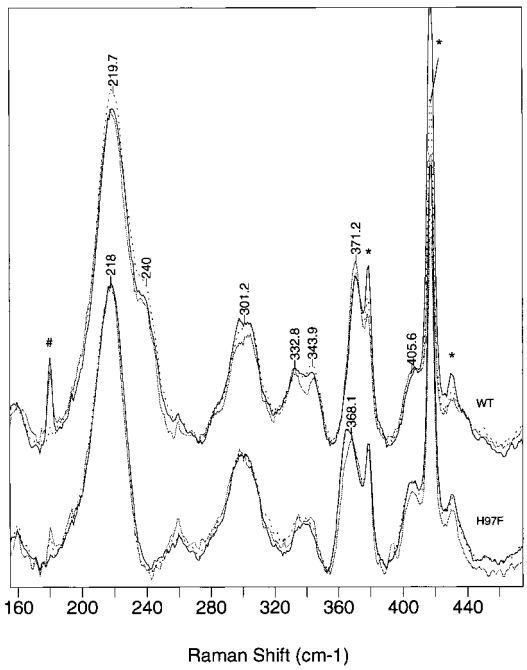

FIGURE 6: Enlarged view of the low-frequency region from 150 to 480 cm^{-1} of the visible resonance-enhanced Raman spectra of the CO photoproduct at 10 ns of the WT and H97F mutant swMb's at pH 7.4 (solid line), 6.2 (dotted line), and 5.1 (gray line) 0.10 M phosphate buffer. Peak markings for WT spectra are for pH 7.4 and are the same as in Figure 4. Details are as in the Methods section.

unchanged within the fitting error by the proximal mutations with the exception of the F-swap mutant. The rather extensive mutations along the F-helix in this protein have resulted in no change in the observed geminate-rebinding rate ($(1.2 \pm 0.2) \times 10^7$ s^{-1}) relative to that for the WT protein ($(1.44 \pm 0.4) \times 10^7$ s^{-1}), but this mutation does result in an increase in the geminate yield (15% for the F-swap mutant versus ~5% for WT protein). Despite the similarity of the fitting results for the single and double mutants, a plot of the actual data clearly indicates that there are some discernible differences in the percent geminate yield. For example,

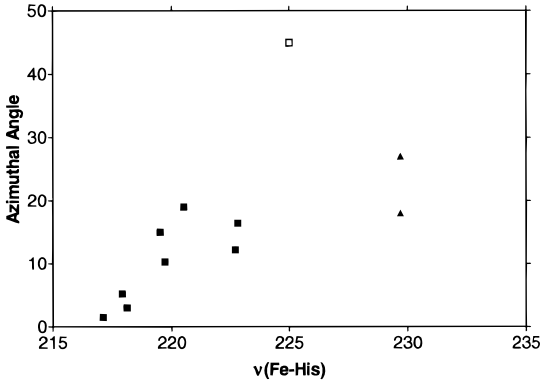

FIGURE 7: Plot of the Mb* photoproduct ν(Fe−His) frequency at the point of maximum intensity of the band profile versus His93 azimuthal angle, ϕ, for the proximal mutants (solid squares) as determined by the molecular modeling calculations (values also tabulated in Table 1) (*32*, *34*). Points for the individual α and β chains within the HbA tetramer (triangles) and for the H93G(Im) myoglobin mutant (open square) are also included.

at times greater than ~2 μs, there is a clear separation of approximately 0.5% between the normalized signals for the WT, H97F, and S92A proteins (data not shown).

Molecular Modeling Results and Correlations with ν(Fe−His). In an effort to relate the spectroscopic variables to the proximal pocket geometry and the kinetic rates, several correlations were explored. The molecular modeling results provide some insight into the structural parameters of the heme pocket for the CO ligated state and also give an estimate to the only parameter that seems to correlate with the ν(Fe−His) frequency: the His 93 imidazole azimuthal angle, ϕ. Values for ϕ (measured herein as the dihedral angle between the imidazole $N_\epsilon-C_\epsilon$ and the $Fe-N_4$ bonds) from the modeling are shown in Table 1 and are plotted in Figure 7 versus the frequency of ν(Fe−His) at maximum intensity for the Mb* derivatives. To further emphasize this correlation, data are also included for the α and β chains within human hemoglobin (HbA tetramer) and the H93G(Im) myoglobin system described below. The peak frequency of the ν(Fe−His) band in the proximal mutants did not correlate

with the observed geminate-rebinding rate, k_{obs}, the geminate yield, or the small changes in the tilt angle of the His93 imidazole ring with respect to the heme normal as determined in the modeling simulations.

DISCUSSION

Much effort has been expended in understanding the structural parameters that control ligand binding to hemoglobins and myoglobins, particularly the identification of the structural motifs on both sides of the heme that contribute to the barriers encountered by a ligand as it enters the protein and then subsequently binds to the iron. The size of the inner barrier, which partially controls the binding of the ligands from within the heme pocket, is related to the energy expenditure required to bring the iron atom back into the heme plane from its out-of-plane position in the 5-coordinate structure. This work done on the iron during ligation is strongly related to the geometry and dynamics of the proximal histidine imidazole ring, which in turn is influenced by changes in the position of the F-helix, the hydrogen-bonding network to other residues within the pocket, and the steric environment produced by the van der Waals packing of the atoms under and against the heme group.

Barrick (*41*) has removed the connection to the F-helix in the His93Gly (H93G) mutant in sperm whale Mb. In this protein an exogenous imidazole molecule can be bound to the iron as a proximal ligand where it functions as a His93 imidazole ring severed from the F-helix. Studies on this system show that relative to the WT protein, the H93G(Im) mutant has increased geminate- and bimolecular-binding rates (*42*, *43*), a rotation of the imidazole ring to an uneclipsed geometry ($\phi \sim 45°$) (*41*), and an increase in the ν(Fe−His) peak frequency to $\sim$225 cm^{-1} (*44*), a value much higher than in WT Mb, but not as high as in the CO photoproduct of HbA at 10 ns. These results demonstrate that despite the near lack of movement of the F-helix upon ligand binding, the bond between the helix backbone and the imidazole ring is crucial to defining the functional properties of Mb.

It remains unclear whether the proximal imidazole ring in H93G(Im) has adopted a new equilibrium geometry solely because of a release of static tension imparted to it by the bond to the F-helix or because additional forces on the ring are also present due to steric interactions or the hydrogen-bonding network. The Raman and kinetic data presented herein address this issue by revealing the effects of a direct disruption of the hydrogen-bonding network through changes in the amino acid sequence via mutagenesis. Regardless of whether the proximal bond to the F-helix is present, if the hydrogen-bonding network plays a large role in controlling the proximal cavity geometry, then elimination of one or more of these bonds should produce a change in the orientation of the imidazole ring, which is typically characterized by the tilt angle with respect to the heme normal, θ, and the rotation angle with respect to the heme pyrrole N_2 and N_4 nitrogens, ϕ. A change in either of these angles can change the amount of steric hindrance between the imidazole C_δ and C_ϵ carbons and the heme pyrrole N_2 and N_4 nitrogens, modulating how far the iron moves out of plane and the strength of the Fe−His covalent bond. This change in the Fe−His bond can be measured spectroscopically as a change in the frequency of the ν(Fe−His) band in the Raman spectrum. Previous work has demonstrated that a decrease in the ν(Fe−His) band is correlated with an increase in the inner barrier and therefore also with a decrease in both the geminate rebinding in a photolyzed sample and the bimolecular binding to a deoxy sample (*14*, *45*−*47*).

Raman. The Raman spectra presented here are resonantly enhanced through the Soret transition of the heme and are thus useful in monitoring changes in the protein that result in changes of the local heme environment. The striking similarity between both the deoxy and Mb* (CO photoproduct at 10 ns) spectra of each protein as well as the spectra between the different proteins (Figures 2 and 3) strongly suggests that neither ligation nor the proximal mutations produce large changes in the globin structure, but that both do result in changes within the heme pocket. The largest changes that are apparent in the Raman spectra occur primarily in the low-frequency region between 180 and 410 cm^{-1} (Figure 3).

ν(Fe−His) Mode. The frequency difference between the Mb* and deoxy ν(Fe−His) bands is indicative of the amount of relaxation that the Mb* species has yet to undergo in order to reach the deoxy endpoint. The small shift of the ν(Fe−His) band in the 10 ns WT Mb* spectrum from the deoxy position in conjunction with the similarity of the Mb* and deoxy 300−375 cm^{-1} propionate sensitive bands suggests either that the conformation of the CO derivative is very similar to that of the deoxy species or that a subnanosecond relaxation has occurred that is missed on the 10 ns time scale of this experiment. In the mutant 10 ns Mb* spectra, the frequency shift of the ν(Fe−His) band peak position from the corresponding deoxy position is not significantly changed from the $\sim$1 cm^{-1} value seen in the WT protein (Figure 3 and Table 1), indicating that the elimination of proximal hydrogen bond(s) in these mutants does not cause a significant decrease in the relaxation rate from the Mb* state to the deoxy state. The decrease in the Mb*-deoxy ν(Fe−His) frequency difference in some of these proteins suggests that either the relaxation following photolysis is slightly faster in these particular mutants or they exhibit less of a departure from the deoxy state upon ligation.

It is interesting to note that the frequency difference between the deoxy and Mb* ν(Fe−His) bands for the F-swap mutant is comparable to that seen in the WT and in the other mutants, indicating that the simultaneous mutation of 8 residues has not resulted in a dramatically larger structural difference between these two states. The observed difference of $\sim$1.1 cm^{-1} is much smaller than the $\sim$5 cm^{-1} difference observed in the isolated α and β chains of human HbA and smaller yet than the $\sim$15 cm^{-1} difference in the intact HbA tetramer. This implies that the 8 residue length of F-helix in the β chains that replaced the corresponding segment in the swMb does not by itself come close to imparting hemoglobin-like behavior to Mb. Despite this seemingly minimal perturbation to the protein structure by the F-swap mutation, the rebinding kinetics indicate that the functional properties have been significantly altered (vide infra).

Raman data taken with more time resolution at room temperature on WT protein in buffer solutions indicate that the ν(Fe−His) frequency does not shift significantly between 30 ps and 10 ns, and that at only a few picoseconds the ν-(Fe−His) band is already very close to the equilibrium deoxy frequency (*48*, *49*). However, cryogenic studies below $\sim$180

K (*50*) and room-temperature studies in high-viscosity solvents, such as high-percentage glycerol solutions and trehalose glasses (*51*) reveal an increase in the ν(Fe−His) frequency by several wavenumbers in the 10 ns CO photoproduct, indicating that the Mb* structure under these conditions does in fact differ from that of the deoxy state and that this is discernible in the Raman spectrum. Cryogenic X-ray studies on the Mb*CO photoproduct have shown that the photoproduct structure is midway between the CO and deoxy structures (*52*), and a time-resolved X-ray study at room temperature indicates that the iron is fully out of plane within a few nanoseconds (*53*). These results strongly indicate that there is in fact a fast component in the proximal relaxation of Mb* at room temperature in buffer solutions. Near-IR transient absorption measurements have also confirmed that the relaxation dynamics of Mb* begin on the subnanosecond time scale (*54*)

The rapidity of the downshift of the ν(Fe−His) band at room temperature and the similarity of the F-helix position in the WT CO and deoxy X-ray structures suggest that the entire proximal relaxation must involve rearrangements that are small in scale and probably localized to small movements of the proximal imidazole ring, the residues involved in the hydrogen-bonding network, a portion of the F-helix, and the heme iron, yet these changes cannot be totally internal motions since changes in bulk viscosity have a dramatic effect on their relaxation dynamics. Likewise, the changes observed in the low-frequency Raman spectra of the mutants must also be due to small changes in the proximal geometry (vide infra).

In an effort to use the current data to better define the changes that do occur as a result of the mutations in the proximal pocket, the ν(Fe−His) band in the Mb* spectra was examined in more detail through a curve-fitting analysis. Previous attempts to characterize the profile of the ν(Fe−His) band in a number of hemoglobin and myoglobin spectra have demonstrated that it is most likely inhomogeneously broadened and have suggested that this broadening is due to conformational heterogeneity (*55*, *56*). We have followed a similar procedure here to fit the 10 ns CO photoproduct spectra for the WT and mutant proteins, as was described above in the Methods section.

While the experiments done herein cannot be used to determine the exact distribution of the proximal substates, some characteristics of it are apparent from the ν(Fe−His) data. Since the profile of the band is not symmetric, the distribution is not Gaussian in energy, which means that the Voigt line shape is not appropriate. The nearly identical widths of the deoxy and Mb* spectra indicate that the distribution of substates in the two ligation states is much the same. If it is assumed that the width of the individual subcomponents is on the order of 16 cm^{-1} fwhm, a width comparable to widths of the heme stretching modes, then the lack of inflection points (i.e., no discernible shoulders) on the ν(Fe−His) band profile suggests that the substate distribution must consist of at least three separate populations or a very broad continuous distribution in order to account for the total width of the band.

Differences in the individual subcomponent bands between the fit solutions for the different protein spectra, whether in frequency or in amplitude, should be viewed as changes in that part of the conformational distribution that gives rise to that particular frequency. It is helpful to interpret the separate components in the fits as one of two limiting cases. It could be that the true distribution does in fact have only a few discrete states, as we have represented by the three Lorentzians (plus one Lorentzian for the ν_9 band), or it could be the case that the true distribution is a fairly continuous one, with many very closely spaced states, and that each component in our fit represents a segment of this distribution.

The ν(Fe−His) bands in the L89I, S92A, and F-swap mutants are shifted to higher frequencies. The L89I mutation was supposed to be the smallest perturbation to the proximal pocket; it is the carbonyl of residue 89 that is involved in the hydrogen-bonding network, not the side chain, and the movement of a methyl group to the adjacent carbon on the side chain should be among the most benign of the possible mutations. Nonetheless, the shift in the ν(Fe−His) band from the WT position in this protein is one of the largest seen in these mutants. Two aspects of the shift in ν(Fe−His) in L89I are noteworthy: (1) The shift is only in the components related to ν(Fe−His); the ν_9 band remains unchanged. (2) The shape of the ν(Fe−His) portion remains the same; that is, the relative contributions of each component in the fit are very close to the WT distribution. In contrast, the band profile has changed in the S92A and F-swap spectra. The fitting results for S92A indicate that the subcomponents have the same frequencies as those in WT, but that the population distribution has shifted toward those with a higher frequency. In the F-swap protein both the relative populations and frequencies have changed.

Given the X-ray data and the lack of large changes in the frequency of ν(Fe−His), it is unlikely that large changes are occurring in the His93 imidazole tilt angle in these mutants. It is more likely that the small changes that are observed are due to slight differences in the rotational angle distribution of the His 93 imidazole ring. Previous NMR results on the cyanomet derivatives of S92A (*29*) and S92D (*30*) showed that the His93 imidazole was rotated ∼5° toward the carbonyl of Leu89, but did not reveal a change in tilt. A small rotation of only ∼5° could be significant in Mb since the orientation of the imidazole ring is close to an eclipsed geometry, and a small change would be significant in relieving the steric forces between the pyrrole 2 and 4 nitrogens and the C_δ and C_ϵ carbons of the imidazole ring. This steric relief would in turn result in a shorter, stronger Fe−His bond and a higher ν(Fe−His) frequency, as is observed for L89I, S92A, and the F-swap mutant (this latter protein is discussed more below).

At this point it is not yet possible to exactly identify the microscopic changes in the proximal pockets of the L89I, S92A, and F-swap mutants that would give rise to the increased rotation of the His93 imidazole ring and concomitant increase in the ν(Fe−His) frequency. The larger Debye−Waller factors seen in the EXAFS study of Sinclair et al. (*31*) suggest that greater disorder is present in the proximal pocket of the L89I mutant, which they attribute to a larger accessible volume for the imidazole ring due to the change in shape of the side chain at position 89. The fact that the L89I ν(Fe−His) band is higher in frequency than that of the WT but has the same profile as the WT protein, and therefore the same relative contribution of each subpopulation to the ν(Fe−His) band, implies that each subcomponent is rescaled in energy by the same amount. This

further implies that the geometrical change effected by the L89I mutation does not merely result in a redistribution of the population among fixed conformations. In contrast, the altered band shape in the S92A spectrum suggests that the Ala side chain causes a bias in the ensemble toward the higher-frequency conformations with the greater azimuthal angle. Both the NMR and X-ray studies indicate that mutations at the Ser92 site cause at least partial disruption of the His97−heme-7-propionate hydrogen bond and movement of the His97 imidazole out of the pocket. These changes could precipitate movement of the heme moiety within the globin fold and/or of the His93 imidazole ring and thereby change the azimuthal angle.

In addition to changing the steric hindrance between the imidazole ring and the heme group, a rotation of the imidazole ring could change the strength of the hydrogen bonds between its N_δ hydrogen and the L89 carbonyl and the S92 hydroxyl group, which in turn would change the basicity of the imidazole ring. Changes in basicity are known to change the frequency of the ν(Fe−His) mode. An extreme example is found in cytochrome *c* peroxidase (ccp), in which the carboxyl group of Asp235 is hydrogen bonded to the proximal His N_δH. The ν(Fe−His) band in ccp contains two components, one at 233 cm^{-1}, assigned to a conformation with a very strong hydrogen bond to the N_δH on the imidazole ring, and one at 246 cm^{-1}, assigned to a conformation in which a complete proton transfer has occurred from the imidazole to the Asp carboxylate group (*57*). The increased ν(Fe−His) frequencies in ccp are almost certainly due to strong hydrogen bonding, but the WT and proximal mutant Mb proteins studied in this work all involve relatively weak hydrogen bonds to the His93 imidazole. Therefore, the changes in ν(Fe−His) observed in these Mb's are probably primarily due to a change in the rotational angle driven by a change in steric factors, and any change in frequency due to perturbations in electron density via altered hydrogen-bond strength is probably a secondary effect.

The ν(Fe−His) band in the Mb* spectrum of H97F is missing the high-frequency portion as well as the ν_9 shoulder. Visual comparison and the curve-fitting results indicate that the lower-frequency components are essentially the same as in WT, but that the high-frequency component has shifted down in frequency. These large changes in the profile of this band as well as changes in the propionate-sensitive bands (vide infra) suggest that removing the hydrogen bond from the His97 imidazole to the heme 7-propionate causes relatively large changes in the proximal pocket. Removal of the H-bond to the 7-propionate could precipitate movement of the heme and possibly also the S92 side chain and the His93 imidazole to which it is hydrogen bonded. The drop in frequency of the highest-energy component to ∼222 cm^{-1} suggests that the associated population has a more eclipsed imidazole ring geometry. Rotation of the heme away from the L89 carbonyl by ∼3° (smaller ϕ) about a conserved axial His93 axis has been confirmed in an NMR study utilizing NOE resonances from the heme methylene protons (*58*). Atamian et al. (*59*) have previously noted that the heme orientation in swMb is influenced by the peripheral groups. They substituted the heme vinyl groups for acetyl groups and found that the heme slipped further into the pocket, and that the ν(Fe−His) band changed shape and frequency dramatically.

Recent measurements of the enthalpic barrier distribution in the L89I and H97F mutants using temperature derivative spectroscopy (TDS) indicate that the protein conformation with the largest rebinding barrier is absent in L89I and reduced in amplitude in H97F (*33*). Hence, in a buffer solution at room temperature, the WT protein Mb* population would relax fully to the conformation associated with the highest rebinding barrier, but in L89I this conformation is not accessible, so the population would only partially relax to the conformation of the next lowest barrier. The absence of the high-barrier conformation should result in a loss of intensity at the low-frequency edge of the ν(Fe−His) band, resulting in an increase in the frequency in the ν(Fe−His) band peak position. The Raman data for the L89I mutant do not follow this expected result exactly, however. Instead of an intensity loss at the low-frequency edge, the entire ν(Fe−His) envelope, but not the ν_9 shoulder, shifts up in energy to a higher frequency. The H97F mutant should also display an increase in the ν(Fe−His) frequency since its enthalpic barrier distribution is missing a large fraction of the high-barrier conformation, but the ν(Fe−His) band actually shifts to a lower frequency. Other features of the Raman spectrum suggest that more drastic alterations within the heme pocket have occurred in the case of H97F than in L89I (vide infra), so a simple correlation with the barrier distribution is not obvious for H97F.

The S92P Mb* ν(Fe−His) band has shifted to lower frequencies and is lacking the prominent ν_9 shoulder. The curve-fitting results indicate that the frequencies of the individual components decrease, but that the population distribution has shifted somewhat toward the higher-frequency components. These opposing changes in the band shape leave the high-frequency edge close to the WT position. Proline is known to deform an α helix, and in naturally occurring proteins it is usually found at the ends of helices, not the middle. It is likely that the proline at position 92 has caused a shift in the F-helix relative to the heme, and the loss of the hydrogen bond to the 7-propionate in this mutant may contribute to this as well. It is not clear at the moment which changes in the proximal geometry cause the observed changes in the S92P ν(Fe−His) band envelope.

A very interesting effect is seen in the double mutants, H97F−S92A and H97F−S92P: the perturbations of the two mutations at positions 92 and 97 appear to act independently, so their results are additive. Since the shifts in both frequency and amplitude of the individual subpopulations in the single-mutant proteins display opposing trends, it is difficult to ascertain what is occurring in the fitting results for the double mutants on a component-by-component basis. The additive effects of the mutations are most evident by overlapping the ν(Fe−His) bands of the WT, single, and double mutants (Figure 4, parts b and c). To a first approximation, the band shape seems to be primarily determined by the H97F mutation, while the frequency of the band as a whole seems to be more affected by the S92 mutation. The H97F mutation eliminates the high-frequency portion of the band, and the S92A mutation shifts the band profile to higher frequencies. The ν(Fe−His) band in H97F−S92A also appears to be shifted up in frequency, but in comparison to S92A, the high-frequency components are missing and the high-frequency edge is steep as in H97F. The S92P mutation appears to shift the lower-frequency edge

toward lower energy, so the H97F−S92P band appears both to be missing the high-frequency portion and to be broadened toward the low-frequency side.

The ν(Fe−His) band in the Mb* spectrum of the F-swap protein most closely resembles that of S92P and S92A in profile (Figures 3 and 4d). The low-frequency edge of the band in the F-swap spectrum overlaps to a large extent with that of the WT spectrum, but the high-frequency edge has been shifted up in frequency as in S92A. It appears that to a first approximation the changes due to the 8 residue mutation are largely due to the change at position 92 from the Mb Ser to the Hb Leu. The other 7 residue changes, however, must certainly have an effect on the overall pocket geometry and could well alter the orientation of the His 93 imidazole with respect to the heme.

In summary, the mutations at positions 89, 92, and 97 do alter the proximal side of the heme pocket and the Raman results are consistent with previous NMR, X-ray, and EXAFS studies. L89I and S92A mutations appear to give rise to a less eclipsed His93 imidazole geometry, which has an increased ν(Fe−His) frequency and a lower rebinding barrier. The H97F and S92P mutations probably result in a more complicated geometrical change within the pocket, possibly involving a shift of the heme with respect to the globin, likely resulting in more strained geometries with lower ν(Fe−His) frequencies. The double mutants display the compound results of the individual mutations at positions 92 and 97. The fitting results follow these trends, but since an apparent frequency shift can be effected either by shifting the amplitudes of fixed frequency components or by shifting the frequencies of fixed amplitude components, it is at times difficult to know which changes are physically meaningful.

It is still not apparent from all these data, however, what is causing the heterogeneity in the ν(Fe−His) band. With the exception of L89I, all the proximal mutations have altered the shape and the width of the band, but none of them have resulted in as large a frequency shift as is seen in the H93G-(Im) spectrum. The covalent bond to the F-helix must be more important to maintaining the geometry of the proximal pocket than are the hydrogen bonds to the His93 imidazole ring. The small frequency shifts and changes in the ν(Fe−His) band profile upon mutation of positions 89, 92, and 97 are most likely due to changes in the steric packing around the imidazole ring and to movement of the heme relative to the globin pocket rather than to the severing of the hydrogen bonds to the imidazole, per say. Changes in the steric contacts with the His 93 imidazole are suggested by the previous studies on S92 mutants in which the position 92 side chains assume an orientation directed away from the imidazole (*26*, *29*, *30*). These studies also indicate that these mutations change the geometry of the 7-propionate and the His97 imidazole, in some cases such that these groups move out from under the heme, which would affect the environment of the His93 imidazole. The EXAFS Debye−Waller factors for mutations of Leu89 indicate that changes in the volume and size of the side chain at this position can result in increased disorder in this region of the pocket (*31*). The largest changes in the shape and width of the ν(Fe−His) band profile, and thus also of the conformational distribution occur when the hydrogen bond from His97 is removed either directly through the H97F mutation or by imposing disorder in the 7-propionate via mutations at Ser92. The hydrogen bond to the 7-propionate appears to be important in preserving the orientation of the heme within the WT pocket. The ν(Fe−His) band is approximately 25% narrower in the H97F mutant than in the WT (not including the ν_9 shoulder), suggesting that the H97 hydrogen bond helps maintain the structural heterogeneity in the WT pocket.

Finally, it appears that the proximal mutations affect the distribution of proximal conformations, and therefore also the ν(Fe−His) band profile, to varying degrees and that this can be interpreted within a hierarchical framework. If a given mutation only caused a local change that did not perturb the variables that determine the population distribution, then either nothing would occur in the ν(Fe−His) band or perhaps all the substate frequencies might shift by the same amount leaving the ν(Fe−His) band profile unaltered, as is seen in the L89I mutant. If, on the other hand, a mutation perturbed the different conformations in an unequivalent manner, it could cause a redistribution of the population among the conformational substates and/or a differential shift in the frequencies associated with these substates, both of which would change the band profile, as is seen in the S92 and H97 mutants. Thus, a conformational hierarchy exists in which variation in some coordinate gives rise to substates, but that within each of these substates other coordinates can be varied to slightly change the substate attributes. It is not clear whether the coordinate that gives rise to the heterogeneity in the ν(Fe−His) band is within the pocket or whether it is manifest over a longer range in the protein fold.

The L89I mutation causes the entire band to change position while the profile is essentially unchanged, suggesting that the perturbation to the pocket and the globin structure in this case is too small to alter the source of the heterogeneity of the ν(Fe−His) band but that it is large enough to change each subpopulation by the same degree. A possible scenario is that the subpopulations differ slightly in the position of the heme or the His93 imidazole tilt angle, but have nearly the same azimuthal angle. If the L89I mutation causes the azimuthal angle in each subpopulation to increase slightly by approximately the same increment, thus allowing the iron atom to assume a more in-plane position, the result would be the observed increase in the overall band frequency without the change in shape. Presumably, a more impacting mutation at position 89 could disrupt the pocket enough so that changes in the coordinate that defines differences in the substates could occur, and this in turn would result in a concomitant change in the band profile in addition to or in lieu of the changes seen in L89I.

In contrast, the S92A, S92P, and F-swap mutants all exhibit band profiles that are quite different from that of the WT but are similar to each other, differing among themselves only in the overall band positions. This suggests that the lack of a hydrogen-bonding group at position 92 results in both a larger change in the protein conformation than did the L89I mutation and also changes in the population distribution among the substates, which in turn results in changes in the band shape. These mutations should result in markedly different changes in the steric factors within the pocket; S92A introduces an aliphatic group, while S92P likely causes a local disruption of the F-helix, and finally the F-swap mutation changes the entire lining of one side of the pocket, yet the three proteins exhibit remarkably similar

band profiles. This indicates that the coordinate(s) in the hierarchy that define(s) the population distribution is more sensitive to the presence or absence of the hydrogen bond from position 92 to the His93 imidazole than to the character of the 92 side chain, but that the nature of the side chain is what determines the frequency of each subpopulation, much as was the case in L89I versus WT. Similar arguments may apply to the H97F mutation, in which different hydrogen bonds are removed and the ν(Fe−His) band also changes profile. One would predict from the behavior of the S92 mutants that a series of mutations at the 97 position might share the same band profile, but differ in the overall position of the band.

A recent vibronic interaction calculation by Stavrov (*60*) provides an alternative explanation to the changes in the ν(Fe−His) band shape. These results do not exclude the possibility of conformational heterogeneity as well, but suggest that under some conditions the band shape is merely a phenomenon of the nature of the vibronic transition and not a characteristic of the particular protein population. The calculation results indicate that the bandwidth, shape, and position change with temperature due to anharmonicity in the iron−imidazole coordinate. At low temperatures, where only the ground vibrational level is populated, the ν(Fe−His) band would be a single Lorentzian, but at higher temperatures where the $\nu \geq 1$ levels become populated, the ν(Fe−His) band broadens significantly on the lower-frequency side since the anharmonic coupling reduces the vibrational frequency. While this would certainly provide an explanation for band changes with temperature, the Raman data herein were all taken at ~10 °C = 283 K. Since all the mutants have approximately the same ν(Fe−His) frequency, they should all have approximately the same Boltzmann distribution for the vibrational population. At 283 K, $k_BT = 197$ cm^{-1}, so the $\nu = 0$, 1, and 2 vibrational levels would all contain at least 10 percent of the population, enough to be detected easily in the Raman experiment. If the anharmonic coupling strength is strong enough, population of these levels is adequate to effect a large change in the band shape. Within this interpretation, the different mutations would impose geometrical changes within the pocket that would then result in a change in the anharmonic coupling constants, and thus give rise to both a shift and change in the profile of the band. The calculation suggests that small changes in the tilt angle, for example, are sufficient to significantly alter the ν(Fe−His) band. This interpretation does not seem adequate, however, in the case of the L89I band, in the series of S92 bands, or for the H97F band. Recall, that a comparison of the L89I and WT spectra or of the S92P, F-swap, and S92A spectra reveals that the spectra are shifted with respect to each other but do not change in profile. If a band shift is brought about by a change in the anharmonic coupling constants, there must also be a change in the band shape since a change in the constants would change both the relative contribution of each vibrational level to the Raman band intensity and the frequency of each vibrational transition, via a change in the spacing between levels, which in turn would change the vibrational population distribution. The H97F ν(Fe−His) band exhibits a loss of intensity on the high-frequency side of the band, which cannot be reconciled easily with changes in the anharmonic coupling constants. To explain this change in the ν(Fe−His) band, one would have to assume that either the population in the $\nu = 0$ level is less than that in the $\nu = 1$ level, which is not consistent with a Boltzmann distribution, or that somehow the contribution for the $0 \rightarrow 1$ transition is less probable than the $1 \rightarrow 2$ transition in the H97F mutant, for which there is no precedent. It is more straightforward to simply interpret the H97F spectral changes as arising from a relative loss of the conformational subpopulation that is associated with the higher-frequency component in the ν(Fe−His) band envelope. Hence, some of the changes in the mutant spectra profiles from that of the WT can be explained by this model invoking anharmonicity, but in the event of a frequency shift without a profile change or a loss of intensity at the high-frequency band edge, conformational heterogeneity must still be invoked.

γ_7. This peak at ~301 cm^{-1}, assigned to the out-of-plane wag mode involving C_a and C_m, undergoes small frequency shifts and changes in profile in the mutants (Figure 3). The Mb* spectra display a broad featureless peak, while in the deoxy spectra this mode appears as a main peak at ~306 cm^{-1} with a shoulder at ~286 cm^{-1}, indicative of increased disorder. In the F-swap mutant Mb* and deoxy spectra this shoulder is a more defined peak at 288 cm^{-1}. The frequency shifts are not correlated with the movements of other peaks in this region of the RR spectrum, though in the Mb* spectra if the γ_7 peak does shift, it is in the same direction as the ν(Fe−His) band. It is not clear what structural elements in the pocket give rise to this behavior, but the difference in the peak in the Mb* and deoxy spectra indicates that the heme pocket in Mb* is not fully relaxed to the deoxy geometry.

Propionate Sensitive Modes: γ_6, ν_8, ν_9, and $\delta(C_\beta C_c C_d)$. All of these modes are out-of-plane motions involving the pyrrole rings of the heme and/or the substituent groups on the perimeter of the heme, as described above in the Results section. These modes are sensitive to movements of the heme and/or its peripheral groups relative to the globin as well as to changes in the geometry of the heme pocket itself.

The WT and L89I mutants have essentially the same profile in the γ_6 and ν_8 bands, indicating that the heme has not moved in the pocket and that the change in the imidazole position in L89I is not coupled to the substituent groups. All of the rest of the mutants sever the hydrogen bond(s) to the heme 7-propionate. In the spectra of S92A, S92P, and the F-swap mutants, the separation between the γ_6 and ν_8 modes has been increased and the γ_6 peak has lost intensity. The NMR data (vide supra) indicate that the S92 mutations increased disorder in the 7-propionate and that it tends to move out of the heme pocket.

The γ_6 and ν_8 bands in the H97F spectrum, and to some degree in the H97F−S92A and H97F−S92P spectra, appear to have coalesced into a single broad band and have also lost intensity, suggesting that in these proteins the contacts between the peripheral groups on the heme and the pocket have changed significantly, perhaps due to a change in the heme orientation in the pocket as was discussed above with respect to the large changes seen in the H97F mutant ν(Fe−His) bands. It is tempting to use the changes seen in these bands as a marker for the amount of freedom and degree of curvature in the 7-propionate, but comparison with HbA and HbI of *Scapharca inaequivalis* reveals that this correlation is not so simple. In deoxy and CO HbA both heme

propionates are solvent-exposed and in an extended geometry. The deoxy HbA spectrum has a prominent ν_8 band, while in the HbA photoproduct spectrum the ν_8 band is severely diminished in intensity. In both the deoxy and CO derivatives of HbA the 333 cm^{-1} band is missing (γ_6 is shifted up to ~350 cm^{-1} and is very weak (*37*)). In HbI the two propionate groups are curved toward the proximal and distal pockets, as they are in Mb, and in going from the deoxy to the CO structure the number of hydrogen bonds per propionate is reduced by one and the propionate groups become slightly more extended (*61*). The γ_6 and ν_8 bands in the deoxy HbI spectrum are very similar to the WT Mb spectra, but in the 10 ns photoproduct HbI* spectrum ν_8 is not present even though both propionates are involved in hydrogen bonds to nearby amino acid side chains (*62*, *63*).

The only consistent pattern present in these data is that when the two propionates are in a well-defined, and possibly also a curved rather than extended, geometry, then the γ_6 and ν_8 bands are both present, easily discernible, and well separated in frequency in the spectra. As disorder is increased in the propionates, the γ_6 and ν_8 band intensities decrease, though not always in both bands. This conclusion is consistent with previous work on HbA embedded in a trehalose glass (*64*). In this glass the propionates should be much less free to move since they are interacting with a fixed matrix rather than the rapidly fluctuating water in buffer solutions. The 10 ns photoproduct spectrum of HbA*CO embedded in the glass contains two very prominent peaks at 333 and 350 cm^{-1} which are not present in the spectrum of the same intermediate in buffer. It is quite likely that these are the γ_6 and ν_8 bands that have appeared once the heme propionates are restricted in motion. Interestingly, the spectrum of Mb* in trehalose does not show much change in the γ_6 and ν_8 bands (*51*): γ_6 does not change at all and ν_8 only undergoes a few wavenumber increase in frequency. This indicates that the propionates are already fairly well localized in the hydrogen-bonding network present in the WT protein and that they probably do not interact with the glass directly. A further test of this scenario might be possible in the proximal Mb mutants that are lacking one or more hydrogen bonds to the 7-propionate. If water has accessed the proximal pocket in these mutants and is hydrogen-bonded to the propionate, or alternatively if the propionate has swung out of the pocket and into the solvent, then replacement of the water by trehalose should alter the γ_6 and ν_8 bands.

Some of the most interesting and largest changes in the Raman data are seen in the $\delta(C_\beta C_c C_d)$ and ν_9 bands in the mutant spectra. The behavior of these bands in the Mb* and deoxy derivatives is nearly identical. A strong correlation is apparent in the frequencies of these two bands. In Mb if $\delta(C_\beta C_c C_d)$ is at ~370 cm^{-1} or above, then ν_9 appears as a distinct shoulder at 240 cm^{-1} on the ν(Fe−His) band with an area that is ~18% of the composite ν(Fe−His)−ν_9 envelope. On the other hand, when $\delta(C_\beta C_c C_d)$ is below this ~370 cm^{-1} cutoff, the ν_9 band has either blended smoothly into the ν(Fe−His) band envelope or disappears completely. This correlation is also seen in the spectra of HbA, tuna Mb, *Scapharca* HbI, and met Mb. The frequency range of $\delta(C_\beta C_c C_d)$ is from ~364 to ~376 cm^{-1}. In Mb the $\delta(C_\beta C_c C_d)$ band appears at 371 cm^{-1} and ν_9 is a prominent shoulder on the ν(Fe−His) band envelope at 240 cm^{-1} in both the Mb* and deoxy spectra, while in HbA the $\delta(C_\beta C_c C_d)$ band appears at the lower limit, 364 cm^{-1}, and ν_9 is missing in both the HbA* and deoxy spectra. Met Mb has the highest frequencies for both the ν_9 and $\delta(C_\beta C_c C_d)$ bands, 255 and 376 cm^{-1}, respectively. In tuna Mb, the $\delta(C_\beta C_c C_d)$ band appears at ~368 cm^{-1} and the ν_9 band is much reduced, appearing as only a weak shoulder on the edge of the ν(Fe−His) band at ~221 cm^{-1} (*65*). The $\delta(C_\beta C_c C_d)$ band in HbI shifts from 371 cm^{-1} in the deoxy derivative to 364 cm^{-1} in the HbI* spectrum, and a relatively weak ν_9 band is present at 240 cm^{-1} in the deoxy spectrum but is missing in the HbI* spectrum. Interestingly, the ν_9 band in HbI appears at a much reduced intensity than in Mb even though the two have comparable $\delta(C_\beta C_c C_d)$ frequencies. It should be noted that although the correlation between the frequencies of the two bands is clear, it is not a linear relationship. Furthermore, the relative intensities of these two bands must be determined by factors separate from those that determine their frequencies since their intensities do not correlate with each other or with the band frequencies.

The frequencies of the $\delta(C_\beta C_c C_d)$ and ν_9 bands also correlate strongly with the structure of the heme pocket. If the propionates participate in hydrogen bonds with other residues in the pocket, as in Mb and HbI, the $\delta(C_\beta C_c C_d)$ mode tends toward higher frequency, but if the propionates are solvent-exposed, as in HbA, this frequency decreases. In addition, the frequency in a given protein increases as the number of hydrogen bonds to the propionates increases, though there is not a fixed relationship between a given frequency and the number of H-bonds. In deoxy HbI, the propionates participate in 3 or 4 hydrogen bonds to residues in the pocket, and in the CO structure they undergo a rearrangement of hydrogen bonds that results in a net loss of one bond to each propionate. In Mb the deoxy and Mb* structures both have two hydrogen bonds to the 7-propionate and at least one to the 6-propionate, a total number less than is present in HbI*, yet Mb* and Mb have a $\delta(C_\beta C_c C_d)$ frequency greater than that seen in HbI*. It is highly likely that the amount of disorder in the propionate geometry determines the frequency behavior of the $\delta(C_\beta C_c C_d)$ and ν_9 bands and that the frequency is not determined by the actual number of hydrogen bonds, per say. Hydrogen bonds to well-ordered amino acid residues would be more likely to restrict the motion of the propionates than would hydrogen bonds to the more disordered bulk solvent molecules. The behavior of the $\delta(C_\beta C_c C_d)$ band for 10 ns CO photoproducts of HbA (*64*) and Mb (*51*) embedded in a trehalose glass supports this hypothesis, and the interpretation is the same as that stated above for the γ_6 and ν_8 bands: there is no change in Mb* spectra when the protein is embedded in the glass since the propionates are already well localized by the hydrogen-bonding network in the pocket, while for HbA* the decrease in propionate disorder in the glass results in an upshift of the $\delta(C_\beta C_c C_d)$ band from 365 to 367 cm^{-1}. In contrast, the ν_9 band in both HbA* and Mb* in trehalose appears as it does in buffer: for HbA* it is not discernible and for Mb* it is a prominent shoulder on the ν(Fe−His) band. It could also be the case that the very high-frequency ν(Fe−His) band envelope in HbA* masks any changes that have occurred in ν_9.

The behavior of the $\delta(C_\beta C_c C_d)$ and ν_9 bands in the proximal swMb mutant spectra is consistent with the above

correlations. In WT and L89I, the full complement of hydrogen bonds to the 7-propionate is present and the $\delta(C_\beta C_c C_d)$ and ν_9 bands are shifted close to their high-frequency values of 371 and 240 cm^{-1}, respectively. In the mutants missing only the hydrogen bond from position 92 to the 7-propionate (S92A, S92P, and the F-swap), the $\delta(C_\beta C_c C_d)$ is downshifted to approximately ~368 cm^{-1} while the ν_9 band moves down to ~231 cm^{-1} and is not distinguishable from the envelope of ν(Fe−His) without curve fitting. These results on the S92 mutants are consistent with the previous NMR and X-ray studies on the same or similar mutants in which increased disorder in both the His97 residue and the 7-propionate, as well as some movement of the propionate out of the pocket, is observed (*26*, *29*, *30*). H97F is lacking the hydrogen bond from the 97 position, and as a result its Raman spectrum is totally missing the ν_9 band and the $\delta(C_\beta C_c C_d)$ band has shifted down to 366 cm^{-1}. It must be that the proposed movement of the heme in this mutant has created a geometry in which the vibrations associated with the ν_9 mode do not couple to the Soret transition and hence do not appear in the Raman spectrum. An alternative explanation is that the mode has shifted so far under the ν(Fe−His) envelope that it cannot be deconvolved in the curve-fitting procedure. It would be interesting to compare the actual structures of the pockets of this mutant and that of HbI, which also has a Phe group packed under the heme. The double mutants, the H97F−S92A and H97F−S92P, once again demonstrate the additive effect of the two mutations. Both of these mutants lack all hydrogen bonds to the 7-propionate, and in their spectra the $\delta(C_\beta C_c C_d)$ band has shifted further down in frequency (to ~364 cm^{-1}) than in either of the single mutants while the ν_9 band is either missing or downshifted to ~227 cm^{-1}.

A few last observations on the behavior of these two bands: If the heme is removed from the globin and then reintroduced and the equilibrium between the normal and flipped heme orientations is re-established, the area of the ν_9 band decreases by a few percent relative to the total area of the combined ν(Fe−His)−ν_9 band envelope, but none of the other bands, including the $\delta(C_\beta C_c C_d)$ band, change at all. This is further evidence that while the frequencies of the $\delta(C_\beta C_c C_d)$ and ν_9 band are correlated, some other factor contributes to their relative intensities. Lastly, the L89I mutant demonstrates that it is possible to have a shift in the ν(Fe−His) band without a shift in either $\delta(C_\beta C_c C_d)$ or ν_9, but the reverse is quite rare. As was mentioned above, this must be due to the fact that the His93 imidazole linkage can be changed slightly without affecting the whole pocket, but if the heme moves enough to alter the geometry of the peripheral substituents, then it is highly likely that the orientation of the proximal histidine geometry has also been changed. The one exception to this is in the pH dependence of the H97F spectrum which shows a very small shift in the $\delta(C_\beta C_c C_d)$ band upon direct protonation of the propionate carboxylate group but no shift in the ν(Fe−His) band (vide infra). In this rare example, the addition of the proton to the propionate group of this mutant must not alter the local geometry and therefore affects only the Raman mode directly involving the propionate.

pH Dependence of Wild Type and His97Phe. Lloyd et al. (*30*) observed a pH-dependent change in the NMR bands associated with the 7-propionate and nearby protons, though they did not see a peak that could be assigned to the proton being titrated. They measured a pK_a of ~6 for the process and assigned this to the His97 imidazole ring, but it was acknowledged that it could also be the carboxylate group of the propionate. The Raman spectra of the WT and the H97F mutants also exhibit changes with changes in pH. Upon decreasing the pH from 7.4 to 5.1, the overlap between the γ_6 and ν_8 bands changes slightly in the WT Mb* spectra and the intensity of γ_7 decreases slightly (Figure 6), indicating that a minor change does occur in the pocket. There is no change in the frequency of the $\delta(C_\beta C_c C_d)$ band, indicating that the propionate carboxylate is probably not being protonated, since doing so should eliminate one of its hydrogen bonds and cause a shift in the $\delta(C_\beta C_c C_d)$ band. Likewise, the protonation of the His97 nitrogen that is involved in the hydrogen bond to the 7-propionate is also very unlikely as this also would eliminate this hydrogen bond in the same way as does the H97F mutation, which in turn would result in a Raman spectrum with dramatic changes in the ν(Fe−His), ν_9, and $\delta(C_\beta C_c C_d)$ bands. However, protonation of the nitrogen of the His 97 imidazole that is not involved in the H-bond to the 7-propionate could occur without causing a significant effect in the Raman spectrum. On the other hand, if it is the His97 that is being protonated, then the pH-dependent change seen in the frequency of $\delta(C_\beta C_c C_d)$ in the H97F spectrum is somewhat perplexing to explain. The $\delta(C_\beta C_c C_d)$ band in the H97F spectrum shifts to a higher frequency by ~2 cm^{-1} at pH ~5.1 (Figure 6). We propose that in WT it is the nonhydrogen-bonded nitrogen of the His97 imidazole that is protonated and that in the H97F mutant the carboxylate of the 7-propionate is protonated. While the addition of a single proton to the 7-propionate in H97F should not alter the degree of disorder in the propionate geometry, it would change the electrostatic environment of the carboxylate group as if it were involved in a strong hydrogen bond, which should increase the $\delta(C_\beta C_c C_d)$ frequency.

Geminate Recombination Kinetics and Yields. All of the mutants except the F-swap Mb display geminate-rebinding rates and yields that are similar to the WT (Table 1). The bimolecular on and off rates (*58*) are also minimally changed in agreement with the previous studies of Smerdon et al. and Shiro et al. (*26*, *29*). The rebinding rates reported herein (Table 1) are the experimentally observed rates, k_{obs}, and have not been deconvoluted into the true geminate-rebinding rate, k_{21}, and the pocket escape rate, k_{23}, (vide infra).[3] The geminate yield (Table 1) gives a measure of the relative contributions of these two processes to the geminate phase kinetics. As the pocket escape rate increases relative to the true geminate-rebinding rate, the geminate yield will decrease. Despite the apparent lack of change in the fitting parameters with the mutations, an overlap of the data does reveal changes in the geminate yield by as much as a few percent (data not shown). Unfortunately, the changes seen in this manner do not correlate well with the changes

[3] This was not done here since the small geminate yield in these proteins results in a very short geminate phase in the kinetic decay that is difficult to fit accurately. The resulting error bars in the fitting parameters give rise to equally large error bars in the actual geminate rate and escape rate when they are calculated from the experimental rate and yield (vide infra). Thus, this separation does not resolve differences that may exist between the proteins.

observed in the ν(Fe−His) band. Both the H97F and S92A data show an apparent increase in geminate yield with respect to WT, which should correlate with an increase in the ν(Fe−His) frequency, yet by both visual inspection and curve-fitting analysis it is quite clear that the ν(Fe−His) band of H97F is lower in frequency than both WT and S92A. It may be that the observed rate is inadequate for comparison and that a separation of the experimental rates into geminate and escape rates is in fact necessary. A second possibility is that a change within the proximal pocket of some of these mutants, such as the shifting of the entire heme moiety, renders the usual correlation between ν(Fe−His) and the geminate kinetic parameters invalid (i.e., the correlated changes in both the geminate parameters and ν(Fe−His) are too small in these proteins under these experimental conditions to be clearly observed in the presence of other factors that also modulate these two markers by comparable amounts, but in a way that is not well correlated).

In contrast to the small changes the geminate kinetics of the single and double proximal mutants, the large increase in the geminate yield for the F-swap mutant with respect to WT is significant, 15% versus 5%, respectively. Recall that the F-swap mutant contains 8 residues from the β chain F-helix, so it is possible that its heme pocket could undergo conformational changes following photolysis similar to those that take place in the β chain. This possibility is supported by the large increase in the geminate phase in the rebinding kinetics for the F-swap protein, similar to what is seen for the isolated β chain from HbA (*32*, *34*). The F-swap protein kinetics have a rebinding rate, k_{obs}, of 1.2×10^7 s^{-1} and a yield of 15%, while the hemoglobin β chain (β_{PMB}) displays a rate and yield of 0.8×10^7 s^{-1} and 10%, respectively. (β_{PMB} is hemoglobin β chain with *p*-mercuribenzoate bound to the cysteine residues which prevents the formation of the β_4 tetramer and thus keeps the chain in monomeric form.)

Since the geminate yields for the WT and the F-swap proteins differ significantly, it is of value to separate the observed rebinding rate, k_{obs}, into the actual geminate-rebinding rate, k_{21}, and the pocket escape rate, k_{23}. If a three-state model is assumed in which there is a bound state, a photolyzed state with the ligand inside the heme pocket, and a fully dissociated state with the ligand outside the protein in the solvent, then a general kinetic scheme can be written:

$$\mathrm{MbCO} \underset{k_{21}}{\overset{k_{12}}{\rightleftarrows}} \mathrm{Mb::CO} \underset{k_{32}}{\overset{k_{23}}{\rightleftarrows}} \mathrm{Mb} + \mathrm{CO} \qquad (1)$$

If this model is valid, k_{21} and k_{23}, can be calculated from the observed geminate rate, k_{obs}, and the geminate yield reported in Table 1 using the following relationships:

$$k_{obs} = k_{21} + k_{23} \qquad (2)$$

$$\text{geminate yield} = k_{21}/(k_{23} + k_{21}) \qquad (3)$$

Using the fitted values for k_{obs} and the geminate yield from Table 1, the calculated geminate-rebinding rates, k_{21}, for the WT and F-swap proteins are $(6.6 \pm 3) \times 10^5$ and $(18 \pm 5) \times 10^5$ s^{-1}, while the escape rates, k_{23}, are $(1.37 \pm 0.4) \times 10^7$ and $(1.0 \pm 0.2) \times 10^7$ s^{-1}, respectively. These rates clearly indicate that the increase in the geminate yield seen in the F-swap mutant is primarily due to an increase in the geminate-rebinding rate, k_{21}. The escape rate, k_{23}, has undergone a negligible change within the error bars. Furthermore, the higher geminate-rebinding rate, k_{21}, and the higher geminate yield for F-swap protein relative to that in the WT indicates that the inner barrier for ligand rebinding is lower in the F-swap protein than in the WT. This then implies that ligand affinity and conformational changes following CO photolysis are controlled at least to a large degree by the amino acid composition of the F-helix.

The peak frequencies of the ν(Fe−His) band in the deoxy and Mb* F-swap spectra do not differ significantly from those of the WT, which would suggest that the contribution of proximal strain to the inner ligand-rebinding barrier has not been altered in this mutant and therefore that the geminate yield and rates should be comparable to those seen in WT, as is the case with the other proximal mutants studied herein. The fact that the geminate yield has increased dramatically indicates that the correlation between the geminate yield and the ν(Fe−His) frequency either does not hold or has been "renormalized" by the drastic mutation in the F-swap protein. There is some precedence for this renormalization of the amount of geminate yield for a given shift in the ν(Fe−His) band when the system under study is changed substantially. The data presented herein from the single and double mutants indicate that small changes in ν(Fe−His) in the Mb system do not imply large accompanying changes in the geminate yield; whereas, data from the HbA systems on the intact tetramer, $\alpha\beta$ dimer, and the isolated α and β chains indicates that over a range of ∼220−226 cm^{-1} for the ν(Fe−His) frequency, the geminate yield increases rapidly from ∼10% to over 25% (*34*, *51*, *66*). In other words, if the data from the Mb and the Hb systems were plotted, one would find that they lie on two separate curves.

Molecular Modeling Results and Correlations with ν(Fe−His). The energy minimized structures of the proximal mutants show that the His93 imidazole azimuthal angle has changed (Table 1, Figure 7). The 6° increase for S92A is in agreement with Shiro et al. (*29*) as well as with more recent NMR results (*58*). As mentioned above, the frequency at maximum intensity of the ν(Fe−His) band does not correlate with the observed geminate rate, $k_{obs,}$ or with the geminate yield in these mutants, as it does in Hb systems, but the ν(Fe−His) frequency does correlate well with the azimuthal angle. This correlation between the azimuthal angle and the ν(Fe−His) peak frequency supports the hypothesis that increases in the steric hindrance between the His93 carbons and the nitrogens of the heme pyrroles do in fact weaken the Fe−His bond and that the ν(Fe−His) frequency can be used as a marker band for this coordinate. The changes with respect to WT that one would predict in the azimuthal angle for the S92A and H97F mutants based on the ν(Fe−His) frequencies are in agreement with recent NMR studies on the cyanomet derivatives of these two mutants: in S92A the His93 imidazole has rotated by ∼10° toward larger values of ϕ relative to a stationary heme, while in H97F the imidazole has not moved but the heme has rotated by ∼3° such that ϕ decreases (a clockwise rotation of the heme when viewed from the proximal side) (*58*). A further test of this correlation is provided with the H93G-(Im) mutant, in which the imidazole is able to assume a fully uneclipsed configuration and the ν(Fe−His) frequency increases dramatically to 225 cm^{-1}, a value close to what one would expect if the proximal data are extrapolated to

an azimuthal angle of 45° (Figure 7). However, despite the good correlation between the ν(Fe−His) frequency and the azimuthal angle, it must be noted that the small 1−2 cm^{-1} shifts in the ν(Fe−His) frequency in some of the proximal mutant spectra could also be caused by changes in other variables in the pocket (steric, electrostatic, or imidazole tilt, for example), and it is most likely changes in these other coordinates, as well as inaccuracies intrinsic to the molecular modeling, that has resulted in the scatter apparent in the plot shown in Figure 7. The fact that other coordinates can influence the ν(Fe−His) frequency is further indicated in Figure 7 by the inclusion of data points for the individual α and β chains within the CO derivative of the HbA tetramer, in which it is known that the proximal geometry adopts a very relaxed geometry due to the quaternary enhancement mechanism in the fully ligated tetramer (*47*). These two HbA points clearly lie outside the relationship between the ν(Fe−His) frequency and the azimuthal angle indicated by all of the myoglobin points. From these data it is not clear if the F-swap mutation is closer in behavior to myoglobin or hemoglobin. Work in progress utilizing separated α and β chains should lend more insight into these issues (*32*, *51*).

CONCLUSIONS

Mutants of sperm whale myoglobin in which one or two of the proximal hydrogen bonds were eliminated or altered were characterized with visible Raman spectroscopy and geminate-rebinding measurements. The results indicate that this conserved proximal hydrogen-bonding network is most likely not crucial to the function of the protein, but primarily enhances the stability of the proximal pocket and helps prevent heme loss in myoglobin. The relaxation from the CO ligated state to the deoxy state is not dramatically altered on the 10 ns time scale, and future picosecond experiments on cryogenic samples will be done to ascertain whether the fast initial component of this relaxation has changed. In contrast to the single or double proximal mutations, severing the covalent linkage between the heme and the protein, as demonstrated in the H93G(Im) mutant, or a large change in the amino acid composition of the F-helix, such as in the F-swap protein, does have a marked effect on the protein function.

The changes in the Raman spectra that are described for the proximal mutants herein indicate that mutations at positions 89, 92, and 97 produce small changes in the His93 imidazole azimuthal angle, the heme 7-propionate geometry, and the position of the heme within the pocket. These changes are additive in double mutants and appear to occur in a hierarchical fashion. For instance, changes in the heme 7-propionate are almost always accompanied by changes in the His93 azimuthal angle, but changes in the azimuthal angle can occur with no changes in the propionates. A careful analysis of the ν(Fe−His) band indicates that some mutations (e.g., L89I) cause no perturbations to the conformational distribution that is responsible for the inhomogeneity present in this band, thus resulting in a frequency shift without a change in band shape. In contrast, other mutations (e.g., those at positions 92 and 97) result in both a frequency shift and a change in band shape and therefore most likely alter the conformational distribution as well. Finally, it appears that the presence or absence of a given hydrogen bond can define the line shape, but that the overall frequency position of the band is determined by the specific residue at the mutation site, as is seen in the S92 mutant series.

Several propionate-sensitive bands (ν_9 at ∼240 cm^{-1}, γ_7 at ∼300 cm^{-1}, γ_6 at ∼335 cm^{-1}, ν_8 at ∼342 cm^{-1}, and $\delta(C_\beta C_c C_d)$ at ∼370 cm^{-1}) were characterized using the data presented herein and comparisons to previously obtained spectra for other Mb's and Hb's. These bands provide good spectral markers for changes in the environments of both the heme macrocycle and its propionate substituents. A frequency correlation between ν_9 and $\delta(C_\beta C_c C_d)$ is noted for the first time.

Lastly, as an attempt to create a more extensive proximal perturbation, 8 residues in the F-helix of swMb were replaced by the corresponding residues of the β chain of HbA. This mutation resulted in a protein whose CO-rebinding kinetics display a large geminate phase, as is found in the isolated β chain of HbA. The predominant effect of this mutation on the Raman spectrum appears to be that associated with the removal of the S92 residue and its hydrogen bonds to the His93 imidazole and to the 7-propionate.

REFERENCES

1. Balasubramanian, S., Lambright, D. G., and Boxer, S. G. (1993) *Proc. Natl. Acad. Sci. U.S.A. 90*, 4718−4722.
2. Braunstein, D., Ansari, A., Berendzen, J., Cowen, B. R., Egeberg, K. D., Frauenfelder, H., Hong, M. K., Ormos, P., Sauke, T. B., Scholl, R., Schulte, A., Sligar, S. G., Springer, B. A., Steinbach, P. J., and Young, R. D. (1988) *Proc. Natl. Acad. Sci. U.S.A. 85*, 8497−8501.
3. Carver, T. E., Olson, J. S., Smerdon S. J., Kryzwda, S., Wilkinson, A. J., Gibson, Q. H., Blackmore, R. S., Ropp, J. D., and Sligar, S. G., (1991) *Biochemistry 30*, 4697−4705.
4. Collman, J. P., Brauman, J. I., and Doxsee, K. M., (1979) *Proc. Natl. Acad. Sci. U.S.A. 76*, 6035−6039.
5. Egeberg, K. D., Springer, B. A., Sligar, S. G., Carver, T. E., Rohlfs, T. J., and Olson, J. S. (1990) *J. Biol. Chem. 265*, 11788−11795.
6. Lambright, D. G., Balasubrumanian, S., and Boxer, S. G. (1989) *J. Mol. Biol. 207*, 289−299.
7. Lambright, D. G., Balasubrumanian, S., Decatur, S. M., and Boxer, S. G. (1994) *Biochemistry 33*, 5518−5525.
8. Mathews, A. J., Rohlfs, R., J., Olson, J. S., Tame, J., Renaud, J. P., and Nagai, K. (1989) *J. Biol. Chem. 265*, 16573−16583.
9. Nagai, K., Luisi, B., Shih, K., Miyazaki, G., Imai, K., Poyart, C., DeYoung, A., Kuriatkowsky, L., Noble, R. B., Lin, S. H., and Yu, N. T. (1987) *Nature 329*, 858−860.
10. Olson, J. S., Matthews, A. J., Rohlfs, R. J., Springer, B. A., Egeberg, K. A., Sligar, S. G., Tame, J., Renaud, J. P., and Nagai, K. (1988) *Nature 336*, 265−266.
11. Olson, J. S., and Phillips, G. N., Jr. (1997) *J. Biol. Chem. 271*, 17593−17596.
12. Springer, B. A., Egeberg, K. D., Sligar, S. G., Rohlfs, R. J., Mathews, A. J., and Olson, J. S. (1989) *J. Biol. Chem. 264*, 3057−3060.
13. Friedman, J. M. (1985) *Science 228*, 1273−1280.
14. Friedman, J. M. (1994) *Methods Enzymol. 232*, 205−231.
15. Perutz, M. F., Fermi, G., Luisi, B., Shaanan, B., and Liddington., R. C. (1987) *Acc. Chem. Res. 20*, 309−321.
16. Perutz, M. F. (1989) *Q. Rev. Biophys. 22*, 139−236.
17. Paoli, M., Dodson, G., Liddington, R. C., and Wilkinson, A. J. (1997) *J. Mol. Biol. 271*, 161−167.
18. Baldwin, J. M., and Clothia, C. (1979) *J. Mol. Biol. 129*, 175−207.
19. Takano, T. (1977) *J. Mol. Biol. 110*, 569−584.
20. Kuriyan, J., Wilz, S., Karplus, M., and Petsko, G. A. (1986) *J. Mol. Biol. 192*, 133−154.
21. Cheng, X., and Shoenborn, B. P. (1991) *J. Mol. Biol. 220*, 381−399.

22. Oldfield, T. J., Smerdon, S. J., Dauter, Z., Petratos, K., Wison, K. S., and Wilkinson, A. J. (1992) *Biochemistry 31*, 8732−8739.
23. Evans, S. V., and Brayer, G. D. (1990) *J. Mol. Biol*. *213*, 885−897.
24. Yamamoto, Y., Nanai, N., Chujo, R., and Suzuki, T. (1990) *FEBS Lett*. *264*, 113−116.
25. Takano, T. (1977) *J. Mol. Biol*. *110*, 537−568.
26. Smerdon, S. J., Krzwda, S., Wilkinson, A. J., Brantley, R. E., Jr., Carver, T. E., Hargrove, M. S., and Olson, J. S. (1993) *Biochemistry 32*, 5132−5138.
27. Mims, M. P., Porras, A. G., Olson, J. S., Noble, R. W, and Peterson, J. A. (1983) *J. Biol. Chem. 258*, 14219−14232.
28. Gibson, Q. H., Wittenberg, J. B., Wittenberg, B. A., Bogusz, D., and Appleby, C. A. (1989*) J. Biol. Chem*. *264*, 100−107.
29. Shiro, Y., Iizuka, T., Marubayashi, K., Ogura, T., Kitagawa, T., Balasubramanian, S., and Boxer, S. G. (1994) *Biochemistry 33*, 14986−14992.
30. Lloyd, E., Burk, D. L., Ferrer, J. C., Maurus, R., Doran, J., Carey, P. R., Brayer, G. D, and Mauk, A. G. (1996) *Biochemistry 35*, 11901−11912.
31. Sinclair, R., Hallam, S., Chen, M., Chance, B., and Powers, L. (1996) *Biochemistry 35*, 15120−15128.
32. Chien, E. Y. T., Kolczak, U., Sligar, S. G., and La Mar, G. N. (1998) *Biochemistry* (submitted for publication).
33. Abadan, Y., Chien, E. Y. T., Chu, K., Eng, C. D., Nienhaus, G. U., and Sligar, S. G. (1995) *Biophys. J. 68*, 2497−2502.
34. Chien, E. Y. T. (1996) in *Role of Proximal Residues in Controlling CO Binding Reactions in Myoglobin*, Ph.D. Thesis, University of Illinois, Urbana-Champaign, pp 16−22, 34−35.
35. Springer, B. A., and Sligar, S. G. (1987) *Proc. Natl. Acad. Sci. U.S.A. 84*, 8961−8965.
36. McLean, M. A., Yeom, H., and Sligar, S. G. (1996) *Biochim. Biophys. Acta 76*, 700−705.
37. Jayaraman, V., and Spiro, T. G. (1996) *Biospectroscopy 2*, 311−316.
38. Hu, S., Smith, K. M., and Spiro, T. G. (1996) *J. Am. Chem. Soc. 118*, 12638−12646.
39. Choi, S., and Spiro, T. G. (1983) *J. Am. Chem. Soc 105*, 3683−3692.
40. Argade, P., Sassaroli, M., Rousseau, D. L., Inubushi, T., Ikeda-Saito, M., and Lapidot, A. (1984) *J. Am. Chem. Soc*. *106*, 6593−6596.
41. Barrick, D. (1994) *Biochemistry 33*, 6546−6554.
42. DePillis, G. D., Decatur, S. M., Barrick, D., and Boxer, S. G. (1994) *J. Am. Chem. Soc. 116*, 6981−6982.
43. Franzen, S., and Boxer, S. G. (1997) *J. Biol. Chem*. *272*, 9655−9660.
44. Franzen, S., Decatur, S. M., Boxer, S. G., Dyer, R. B., Woodruff, W. H. (1996) *Proceedings of the Fifteenth International Conference on Raman Spectroscopy* (Stein, P., and Asher, S. A., Eds.) pp 66−67, The McGraw-Hill Companies, Inc., New York. Note: the value of 228 cm^{-1} for the ν(Fe−Im) frequency in this work should be 225 cm^{-1} and was inaccurately reported due to a calibration error (S. Franzen, personal communication).
45. Rousseau, D. L., and Friedman, J. M. (1988) *Biological Application of Raman Spectroscopy* (Spiro, T. G., Ed.) Vol. III, pp 133−215, Wiley & Sons, New York.
46. Kitagawa, T. (1988) *Biological Application of Raman Spectroscopy* (Spiro, T. G., Ed.) Vol. III, pp 97−131, Wiley & Sons, New York.
47. Peterson, E. S., and Friedman, J. M. (1998) *Biochemistry 37*, 4346−4357.
48. Findsen, E. W., Scott, T. W., Chance, M. R., and Friedman, J. M. (1985) *J. Am. Chem. Soc. 107*, 3355−3357.
49. Franzen, S., Bohn, B., Poyart, C., and Martin, J. L. (1995) *Biochemistry 34*, 1224−1237.
50. Ahmed, A. M., Cambell, B. F., Caruso, D., Chance, M. R., Chavez, M. D., Courtney, S. H., Friedman, J. M., Iben, I. E. T., Ondrias, M. R., and Yang, M. (1991) *Chem. Phys. 158*, 329−351.
51. Peterson, E. S., and Friedman, J. M. (1998), unpublished results.
52. Schlicting, I., Berendzen, J., Phillips, G. N, Jr., and Sweet, R. M. (1994) *Nature 371*, 808−812.
53. Šrajer, V., Teng, T., Ursby, T., Praderv&, C., Ren, Z., Adachi, S., Schildkamp, W., Bourgeois, D., Wulff, M., and Moffat, K. (1996) *Science 274*, 1726−1729.
54. Jackson, T. A., Lim, M., and Anfinrud, P. A. (1994) *Chem. Phys*. *180*, 131−140.
55. Gilch, H., Schweitzer-Stenner, R., and Dreybrodt, W. (1993) *Biophys. J*. *65*, 1470−1485.
56. Gilch, H., Dreybrodt, W., and Schweitzer-Stenner, R. (1996) *Biophys. J. 69*, 214−227.
57. . Smulevich, G., Mauro, J. M., Fishel, L. A., English, A. M., Kraut, J., and Spiro, T. G. (1988) *Biochemistry 27*, 5477−5485.
58. Wu, Y., Chien, E. Y. T., Sligar, S. G., and La Mar, G. N. (1998) *Biochemistry 37*, 6979−6990.
59. Atamian, M., and Bocian, D. (1987) *Biochemistry 26*, 8319−8326.
60. Stavrov, S. (1997) *Biochim. Biophys. Acta* (submitted for publication).
61. Royer, W. E., Jr. (1994) *J. Mol. Biol. 235*, 657−681.
62. Rousseau D. L., Song S., Friedman, J. M., Boffi, A., and Chiancone, E. (1993) *J. Biol. Chem. 268*, 5719−5723.
63. Royer, W. E., Jr., Pardanani, A., Gibson, Q. H., Peterson, E. S., and Friedman, J. M. (1996) *Proc. Natl. Acad. Sci. U.S.A. 93*, 14526−14531.
64. Gottfried, D. S., Peterson, E. S., Sheikh, A. G., Wang J., Yang, M., and Friedman, J. M. (1996) *J. Phys. Chem. 100*, 12034−12042.
65. Vidugiris, G. J. A., and Friedman, J. M., unpublished results.
66. Kwiatkowski, L. D., Hui, H. L., Wierzba, A., Noble, R. W., Walder, R. Y., Peterson, E. S., Sligar, S. G., and Sanders, K. (1998) *Biochemistry 37*, 4325−4335.

BI980752U